HHS Public Access

Author manuscript

Nat Immunol. Author manuscript; available in PMC 2022 August 04.

Published in final edited form as:

Nat Immunol. 2021 November ; 22(11): 1440–1451. doi:10.1038/s41590-021-01048-3.

Mitochondrial Complex II In Intestinal Epithelial Cells Regulates T-cell Mediated Immunopathology

Hideaki Fujiwara[1,#], **Keisuke Seike**[1,#], **Michael D. Brooks**[1], **Anna V Mathew**[2], **Ilya Kovalenko**[3], **Anupama Pal**[4], **Ho-Joon Lee**[3], **Daniel Peltier**[5], **Stephanie Kim**[1], **Chen Liu**[6], **Katherine Oravecz-Wilson**[1], **Lu Li**[1], **Yaping Sun**[1], **Jaeman Byun**[2], **Yoshinobu Maeda**[8], **Max S. Wicha**[1], **Tom Saunders**[7], **Alnawaz Rehemtulla**[4], **Costas A Lyssiotis**[3], **Subramaniam Pennathur**[2], **Pavan Reddy**[1,*]

[1]Department of Internal Medicine, Division of Hematology and Oncology, University of Michigan, Rogel Cancer Center, Ann Arbor, MI, USA.

[2]Department of Internal Medicine, Division of Nephrology, University of Michigan Health System, Ann Arbor, MI, USA.

[3]Department of Molecular and Integrative Physiology, University of Michigan, Ann Arbor, MI 48109, USA.

[4]Department of Radiation Oncology, University of Michigan, Ann Arbor, MI, USA.

[5]Department of Pediatrics, Division of Hematology/Oncology and BMT, University of Michigan Health System, Ann Arbor, MI, USA.

[6]Department of Pathology and Laboratory Medicine, Rutgers-Robert Wood Johnson Medical School, New Brunswick, NJ, USA.

[7]Transgenic Animal Model Core, University of Michigan Medical School, Ann Arbor, Michigan, USA.

[8]Department of Hematology Oncology and Respiratory Medicine, Okayama University Graduate School of Medicine, Dentistry, and Pharmaceutical Sciences, Okayama, Japan.

Abstract

Intestinal epithelial cell (IEC) damage by T cells contributes to graft-versus-host disease (GVHD), inflammatory bowel disease (IBD) and immune checkpoint blockade (ICB) mediated colitis. But little is known about the target cell intrinsic features that influence disease severity. Herein we identified disruption of oxidative phosphorylation and an increase in succinate levels in the

[*]**Corresponding Author:** Pavan Reddy, Department of Internal Medicine, Division of Hematology and Oncology, Blood and Marrow Transplantation Program, University of Michigan Rogel Cancer Center, 3110 Rogel Cancer Center, 1500 E. Medical Center Drive, Ann Arbor, MI 48105-1942, USA, reddypr@med.umich.edu. Tel.: +1-734-647-5954, Fax: +1-734-647-9271.

[#]These authors contributed equally.

Author contributions: H.F. and P.R. conceived and designed this study. H.F., K.S. and P.R. planned and guided the research and wrote the manuscript. H.F., K.S., I.K., A.V.M., A.P., H.M., T.T., I.H., S.J.W., S.K., A.T., D.S., K.O.W., Y.S., and J.B. performed experiments. I.K., A.V.M., H.J.L. and J.B.analyzed LC/MS and MFA data. D.P. performed experiments, analyzed human data and edited the paper. C.L. performed experiments and histopathological analysis. M.D.B performed transcriptome analysis. H.F., T.S. and P.R. generated the *SDHA* floxed mice. P.S., Y.M., M.S.W., T.S., C.A.L., S.P., A.R. and R.P. supervised the work carried out in this study.

Conflict of interest statement: The authors have no conflict of interest.

IECs from several distinct in vivo models of T cell mediated colitis. Metabolic flux studies, complemented by imaging and protein analyses identified disruption of IEC intrinsic succinate dehydrogenase A (SDHA), a component of mitochondrial complex II, in causing these metabolic alterations. The relevance of IEC intrinsic SDHA in mediating disease severity was confirmed by complementary chemical and genetic experimental approaches and validated in human clinical samples. These data identify a critical role for the alteration of the IEC specific mitochondrial complex II component SDHA in the regulation of the severity of T cell mediated intestinal diseases.

Keywords

mitochondria; succinate dehydrogenase; bone marrow transplantation; graft-versus-host disease; intestinal epithelium

INTRODUCTION

The non-infectious inflammatory diseases that occur in the intestinal tract such as autoimmune inflammatory bowel diseases (IBD), immune checkpoint blocker (ICB) mediated colitis, and alloimmune T cell mediated gastrointestinal graft-versus-host disease (GI-GVHD) often have similar symptoms and cause significant morbidity and mortality [1 2 3]. Although the pathophysiology of each of these diseases is a complex interplay of the environmental and genetic factors, T cell mediated damage of IECs plays a vital role in the cause and severity of all of these conditions. T-cell immunosuppression with corticosteroids, and anti-cytokine therapies have shown good results with adverse effects, but are still incomplete [5 7 8]. Thus the biology and treatments of these diseases are often understood and targeted from the immune cell perspective, but the pathogenesis and severity from the target cells, the intestinal epithelial cells (IECs) perspective remain undefined. Mitochondria are critical hubs of cellular metabolism and bioenergetics, namely oxidative phosphorylation (OXPHOS). Emerging data in recent years have brought into focus the central role of immune cell metabolism in the regulation of intestinal inflammatory diseases. Specifically, antigen-presenting cells (APCs), including macrophages and dendritic cells, and T cells show changes in metabolic programming, including morphological alterations in mitochondria, transitioning from glycolysis dependence (pro-inflammatory macrophages and effector T cells) to OXPHOS dependence (anti-inflammatory macrophages and memory T cells) [9 10 11]. The metabolic shifts in immune cells contribute to severity of T cell mediated diseases such as GI GVHD and IBD. However, whether the metabolism of the targets of these pathogenic T cells in these diseases, the IECs, are perturbed or reprogrammed, and if so, whether this has an impact on the disease severity remains unknown. The mammalian GI tract is a relatively hypoxic region and interfaces with microbiome and therefore IEC metabolism is uniquely adapted to its environment [12 13]. It remains unknown whether the IECs have the ability to adapt their metabolic programs to develop tolerance against inflammation mediated damage.

In this study, we aimed to determine the metabolic changes in IECs when they are targeted by pathogenic T effector cells. Herein we report that in the context of pathogenic T

cell mediated damage, the IECs demonstrated a reduction in OXPHOS and accumulated succinate as a result of decrease in SDHA, a component of mitochondrial complex II. The reduction in IEC intrinsic SDHA aggravated disease severity in multiple T cell mediated models of intestinal damage such as GI GVHD, IBD and ICB mediated colitis. Further mechanistic studies demonstrated that the disruption of mitochondrial complex II by the reduction of SDHA in the IECs was caused by their direct contact with the cytotoxic T cells (CTLs). Finally, the results were validated in human samples of GI GVHD demonstrating that IEC intrinsic metabolism regulates T cell mediated intestinal disease severity.

Results

Analysis of mitochondrial respiration in IECs

We explored the impact of immune mediated attack on the bioenergetics of IECs utilizing well-established lethally irradiated MHC disparate BALB/c into WT B6 model of GVHD. $CD326^+$ IECs from un-transplanted naïve B6 animals, the syngeneic, and allogeneic animals were harvested 21 d after hematopoietic stem cell transplantation (HCT) and their bio-energetic profiles were analyzed with Seahorse XF^4. Compared with IECs from naïve and syngeneic animals, IECs from allogeneic animals demonstrated significantly lower oxygen consumption rates (OCR), but similar extracellular acidification rates ECAR and reduced OCR/ECAR ratio (Fig. 1a–c). IECs from allogeneic animals responded poorly to treatment with carbonyl cyanide-p-trifluoromethoxyphenylhydrazone (FCCP) when compared to IECs from syngeneic animals (Fig. 1b) despite demonstrating similar viability (Extended Data Fig. 1a). The maximal respiratory capacity and reserve capacity of IECs from allogeneic animals were also significantly reduced (Extended Data Fig. 1b) but the cell surface oxygen consumption, non-mitochondrial -did not significantly change with addition of NADH (Extended Data Fig. 1c).

Next, we assessed the activity of the various mitochondrial complexes to determine the potential reasons for the reduction of OCR[5]. Allogeneic IECs demonstrated poor responsiveness to succinate, substrate for complex II (Fig.1d), but demonstrated comparable responses to pyruvate/malate and duroquinol, (substrates for complexes I and III, IV respectively) (Fig. 1d and Extended Data Fig. 1d) and in the ability to oxidize NADH to NAD^+ between the groups (Fig. 1e). The net $NADH/NAD^+$ ratio was lower in IECs from allogeneic animals (Fig. 1f) suggesting that complex II function may be the primary cause for altered ETC. Blue Native Polyacrylamide Gel Electrophoresis (BN-PAGE) showed alteration of mitochondrial complex II with no significant changes in other mitochondrial super complex levels (Extended Data Fig. 1e and f).

TCA cycle metabolite profiling in IECs

Because oxidative phosphorylation (OXPHOS) links mitochondrial respiration and Kreb's (TCA) cycle, and complex II is critical for both processes, we next profiled for all of the TCA cycle-related metabolites in the IECs using Liquid chromatography mass spectrometry (LC/MS). Kidneys from the same animals served as controls for non-GVHD target organs. The levels of succinate were significantly elevated, whereas the levels of malate, and fumarate were decreased in the IECs harvested from allogeneic recipients when compared

with naive and syngeneic recipients (Figure 2a and 2b)but not in the control organs, kidneys(Fig. 2c and Extended Data Fig. 1g). The levels of lactate were similar in the IECs from all groups, suggesting a lack of shift or increase in glycolysis (Extended Data Fig. 1h). To further confirm lack of shift from OXPHOS to glycolysis, IECs isolated after HCT were cultured in ^{12}C-glucose or ^{13}C-glucose for 4 h and analyzed for incorporation of ^{13}C into glycolysis and no differences were observed in the incorporation of ^{13}C into lactate between the groups (Fig. 2d).

Mechanisms for increased levels of succinate in the IECs

To explore the mechanisms for succinate accumulation we first determined whether there was a contribution from enhanced anaplerosis or β-oxidation. The syngeneic and allogeneic transplant recipients were administered an oral bolus of ^{13}C-glucose or ^{12}C-glucose (the control) 7 d after HCT and the IECs were harvested 4 h later and analyzed for incorporation of ^{13}C. There was a significant reduction in incorporation of ^{13}C into citrate and malate in the allo-IECs (Fig. 2e). Next, we performed metabolic flux analysis (MFA). IECs were harvested from syngeneic and allogeneic transplant recipients 7 and 21 days after HCT and treated with ^{13}C-glutamine or ^{12}C-glutamine for 4 h.. Similar levels of ^{13}C incorporation were detected in both alpha-ketoglutarate and succinate (Extended Data Fig. 1i).

Further, there were no significant differences in the IEC acylcarnitine levels between the groups (Table. 1). MFA analyses of syngeneic and allogeneic transplant recipients treated with oral ^{13}C-palmitate 7 d after the BMT also demonstrated no significant differences in its incorporation into acylcarnitine (Supplementary Table. 1) or the succinate pools pool (Fig. 2f).

The above data collectively suggested that increased levels of succinate was not from an increase in influx from glucose, glutamine anaplerosis or β-oxidation.

We therefore next hypothesized that high level of succinate is a function of reduction in complex II subunit, the enzyme SDHA, an enzyme that catalyzes the oxidation of succinate to fumarate, and generates $FADH_2$ in ETC. To evaluate SDHA enzymatic activity we stained cryosections of GVHD target organs (colon, ileum, liver, and skin) and non-GVHD target organs (kidney, pancreas, and heart) as controls from the recipients on days 7 and 21 post HCT (Extended Data Fig. 2a, b). SDHA activity was preserved in the liver, skin, kidney, pancreas, and heart in naïve and post HCT tissues, whereas it was significantly reduced in the colon and the ileum post allo-HCT (Figure 2g and Extended Data Fig. 2c). .

Validation of reduction in SDHA

We next examined the level of SDHA and other mitochondrial ETC complex proteins in the IECs.. Significantly reduced SDHA protein levels were observed in allogeneic IECs post HCT (Fig. 3a–b and Extended Datat Fig. 3a–b) whilst other mitochondrial complex II protein such as SDHB, and complexes I and III, showed no significant reduction (Fig. 3a and 3c and Extended Data Fig. 3a–b) [6].

We performed immunofluorescent staining of GI-GVHD lesions and analyzed the fluorescent intensity in an operator blinded manner. The SDHA expression levels were

significantly lower in the intestines from allogeneic animals (Fig. 3d–e). By contrast, the non-GVHD target organs, heart, liver, and kidney demonstrated no differences in the expression of SDHA between the groups (Fig. 3e and Extended Data Fig. 3c). Finally, to definitively demonstrate that the reduction in SDHA is not a consequence of reduction in mitochondria, we stained IECs for SDHA with gold particles post allo-HCT and visualized the gold particles using transmission electron microscopy (TEM). Mitochondria in allogeneic IECs had significantly fewer SDHA gold particles (Fig. 3f and Extended Data Fig. 3d). The IECs of allogeneic animals were also associated with significant blunting and loss of discernable cristae in the mitochondria compared to IECs from syngeneic animals (Extended Data Fig. 3e). The numbers of mitochondria as measured by mitochondrial DNA copy numbers were however similar in the IECs from both groups (Extended Data Fig. 3f).

Reduction of SDHA in T cell mediated colitis

We next explored whether the reduction in SDHA is germane to any type of intestinal damage, or was limited to T cell mediated intestinal damage. First, to rule of strain and model dependence in the induction of intestinal GVHD, we harvested IECs from lethally irradiated MHC-matched, multiple host minor histocompatibility antigens (mHAgs)-mismatched C3H.SW→C57BL/6 model. The IECs from only the allogeneic recipients showed significantly lower SDHA levels as above (Extended Data Fig. 4a and b).
To determine whether irradiation dependent conditioning was critical, we next utilized chemotherapy-based conditioning regimen consisting of treatment with busulfan and cyclophosphamide. The allo-IECs once again demonstrated significantly lower levels of SDHA (Extended Data Fig. 4c and d). Next, to determine whether allorective T cells alone, in the absence of conditioning induced damage, were sufficient to cause reduction in SDHA we utilized the fourth model, MHC-haploidentical, non-irradiated B6→B6D2F1 system.. Allogeneic IECs once again demonstrated significantly reduced levels of SDHA with an increase in levels of succinate (Fig. 4a, b and c).

It is possible that any non-T cell mediated damage of the host IECs could also lead to reduction in SDHA. We irradiated mice with escalating doses to cause intestinal damage but without HCT to induce radiation induced colitis. In contrast to allogeneic T cell mediated colitis model systems, IECs harvested after irradiation did not demonstrate a reduction in SDHA levels nor an increase in succinate levels (Fig. 4d–f).

We next determined whether the reduction of SDHA non-alloreactive T cell mediated immunopathology, such as in autoimmune T cell mediated colitis by transferring WT B6 $CD45RB^{high}$ naïve T-cells into B6 recombination activating gene 1 deficient (*RAG-1*$^{-/-}$) hosts. Twelve weeks after T-cell transfer, IECs were harvested from $CD45RB^{high}$ T-cell recipients and control $CD45RB^{low}$ T-cell recipients and those from the $CD45RB^{high}$ group showed significantly lower levels of SDHA and higher levels of succinate accumulation (Fig. 4g–i).

To further analyze the specificity to T cell mediated damage, we next induced colitis by chemical damage. To this end, we utilized the well-established dextran sulfate sodium (DSS)-chemical induced inflammatory colitis model. In contrast to autoimmune T cell

mediated colitis, colonic IECs from DSS colitis-induced animals demonstrated similar SDHA and succinate levels as the control animals (Extended Data Fig. 4e–g).

Given above, we next hypothesized that reduction of SDHA in IECs will also be applicable to iatrogenic immune checkpoint blockers (ICB) mediated colitis. We utilized the recently developed experimental model for ICB mediated colitis following administration of anti-CTLA-4 antibody.[7,8] Consistent with the hypothesis, treatment with anti-CTLA-4 induced reduction of SDHA with increase in succinate in the IECs(Fig. 4j–l and Extended Data Fig. 4h).

Functional relevance of reduction in SDHA in IECs

We treated primary colonic epithelial cells (PCECs) from B6 WT animals with three well-characterized SDHA inhibitors, namely itaconate, dimethyl malonate and 4-octyl-itaconate [9]. We first determined and then utilized these agents at doses that inhibited SDHA but were not cytotoxic (Fig. 5a–b). SDHA inhibition promoted production of reactive oxygen species (ROS) in the cytoplasm (CellROX; Extended Data Fig. 5a and b) and in mitochondria (MitoSOX; Fig.5c and Extended Data Fig. 5c and d). We also utilized atpenin A5, inhibitor of other components of mitochondrial complex II [10] and found that it also induced similar ROS production (Extended Data Fig. 5e). Similar to PCECs, IECs harvested from the colon and ileum of allogeneic mice showed higher ROS (Extended Data Fig. 5f). In addition mitochondria from syngeneic and naïve animals showed similar levels of ATP production, whereas mitochondria from allogeneic animals produced less ATP, but this difference diminished after malonate treatment (Fig. 5d). Furthermore, allo-IECs showed significantly lower mitochondrial membrane potentials ψm than syn-IECs (Extended Data Fig. 5g), consistent with the defect in mitochondrial respiration and OXPHOS.

We next reasoned that the inhibition of SDHA in the IECs enhanced their sensitivity or permissiveness to T cell mediated cell death. B6 PCECs pre-treated with malonate or itaconate showed significantly higher levels of cell death compared with diluent treated PCECs co-cultured with allo-primed T cells but not in those co-cultured with syngeneic T cells (Fig. 5e, Supplementary Fig. 1a). Pretreatment if PCECs with 4-octyl itaconate also demonstrated similar enhanced susceptibility to allo-T cell mediated cell death (Fig. 5f, Supplementary Fig. 1b).

Because succinate is pro-inflammatory[11] we determined whether succinate by itself affected GVHD severity after HCT. Succinate was orally administrated daily to HCT recipients from day 0 after HCT. We found that there were no differences in the survival rate and GVHD severity (Extended Data Fig. 5h and i). We also harvested IECs from naïve, syngeneic recipient mice and allogeneic recipient mice and analyzed for expression of succinate receptor 1 (SUCNR1). In contrast to macrophages, IECs did not express SUCNR1(Extended Fig. 5j). [12]. These data suggest potential lack of exogenous or paracrine effect by the succinate released from the IECs, but cannot rule out effects on microbiome or macrophages. To assess for potential autocrine effects, we determined the expression of hypoxia inducible factor-1α (HIF1α) and its targeted genes that are known to be induced by succinate[11]. IECs from allogeneic mice showed increased expression of HIF-1α and its target genes such as cytochrome B (Extended Data Fig. 5k) suggesting cell intrinsic

autocrine effects of succinate accumulation. It is nonetheless possible that the change in HIF-1α expression might also be secondary to reduction in local intestinal tissue oxygen levels after allo-HCT. However, allogeneic recipients demonstrated increased levels of oxygen (decreased hypoxia) both in colon and ileum when compared with syngeneic recipients (Extended Data Fig. 5l). We also determined the caseinolytic protease P (ClpP) levels in the IECs after HCT to assess whether they contributed to changes in their levels of mitochondrial complexes in context of changes in oxygen[13 14]. ClpP levels were similar in IECs from both syngeneic and allogeneic recipients (Extended Data Fig. 5m, n).

IEC intrinsic SDHA regulates colitis severity

We examined the role of IEC intrinsic SDHA in regulating in vivo severity of intestinal GVHD. To this end, we took multiple complementary, but distinct approaches. First, we utilized the three distinct chemical inhibitors of SDHA, namely malonate, itaconate and atpenin A5. The oral doses at which they inhibited SDHA function 12 h after *in vivo* administration (Extended Data Fig. 6a) were utilized for analyzing the effect of SDHA inhibition on GI GVHD as in Methods. All of the syngeneic mice survived regardless of treatment, but the allogeneic mice receiving itaconate, malonate or atpenin A5 demonstrated significantly greater mortality and had more severe GVHD than vehicle treated allo-recipients (Fig. 6a–b and Extended Data Fig. 6b). Histopathological analysis confirmed increased GVHD severity in the colon and ileum, but not in the liver, skin, and lungs (Fig. 6c and Extended Data Fig. 6c).

Because chemical inhibitors could have off-target effects, we next utilized genetic models. We first used SDH assembly factor 1 deficient B6 mice (*Sdhaf1*$^{-/-}$) that have 20–50% the SDH activity compared with WT B6 [15 16]as recipients in allo-HSCT. Succinate levels in IECs from *Sdhaf1*$^{-/-}$ B6 mice at baseline were higher than those in IECs of WT B6 mice (Supplementary Fig. 6d). Littermate WT and *Sdhaf1*$^{-/-}$ recipients were utilized to rule out potentially confounding effects from endogenous microbiome changes. Syngeneic WT and *Sdhaf1*$^{-/-}$ animals showed no mortality demonstrating lack of differences in conditioning mediated toxicity. By contrast allogeneic *Sdhaf1*$^{-/-}$ B6 mice showed greater severity and mortality from GVHD when compared with allogeneic WT B6 controls (Fig. 6d and e). Histopathological analysis of the GI tract confirmed greater GVHD severity in the allogeneic *Sdhaf1*$^{-/-}$ mice (Fig. 6f and Extended Data Fig.6e) and the IECs harvested from these animals showed lower SDHA levels than those from allogeneic WT littermates (Fig. 6g and h) along with higher levels of succinate (Fig. 6i).

It is possible that reduction of SDHA in IECs at baseline might make them generally more susceptible to any intestinal damage because of reduced fitness and might not be unique only to T cell mediated pathology. To test this, we induced chemical colitis with DSS in *Sdhaf1*$^{-/-}$ B6 animals and compared severity with B6 WT littermates. The *Sdhaf1*$^{-/-}$ and the WT animals demonstrated similar changes in body weight and colitis severity (Extended Data Fig. 6f).

The above approaches, given the systemic effects, do not distinguish potential confounding effects of SDHA activity in host immune and other cell types from the direct exclusive effects on IECs. Therefore, we next generated BM chimeric mice [WT B6Ly5.2→ Sdhaf1−/

− B6] wherein low SDH activity was restricted to the non-hematopoietic recipient cells and the control [WT B6Ly5.2→ WT B6] and utilized them three months later as recipients of allogeneic HCT. The allogeneic [WT B6Ly5.2→ Sdhaf1−/− B6] chimeras demonstrated significantly shorter survival when compared with WT B6Ly5.2→ WT B6 recipients (Fig. 6j).

Finally, to eliminate germline effects of *Sdhaf1*$^{-/-}$ and to demonstrate that the enhanced intestinal pathology is caused only by deficiency of SDHA specifically and limited to the IECs, we generated IEC specific SDHA deficient B6 animals. To this end we obtained *Sdha* gene trap, floxed it, and then these mice containing loxP-flanked *Sdha* were crossed with *Villin-Cre* mice to generate mice specifically lacking *Sdha* in IECs (*Sdha*$^{\Delta/IEC}$; Extended Data Fig. 6g). Efficient reduction of SDHA exclusively in the IECs was confirmed (Extended Data Fig. 6h and i) in *Sdha*$^{\Delta/IEC}$ mice. Importantly, both the *Sdha*$^{\Delta/IEC}$ and *Sdha*$^{fl/IEC}$ mice expressed similar levels of SDHA protein in the heart, liver, and skin demonstrating enterocyte specific reduction of SDHA (Extended Data Fig. 6j). The WT *Sdha*$^{fl/IEC}$ and IEC specific KO *Sdha*$^{\Delta/IEC}$ littermate animals were utilized as HCT recipients as in Methods. Allogeneic IEC specific KO *Sdha*$^{\Delta/IEC}$ recipients demonstrated significantly greater mortality and clinical severity of GVHD when compared to the allogeneic WT *Sdha*$^{fl/IEC}$ littermate animals (Fig. 6k and l).

Immunoresponsive gene 1 (*Irg1*) enhances endogenous itaconate (inhibitor of SDHA) production [17], thus resulting in increased levels of SDHA. Therefore, we hypothesized that the absence of *Irg1* would result in improved levels of SDHA after allo-BMT and result in reduction in intestinal damage from GVHD. At baseline IECs in *Irg1*$^{-/-}$ mice showed similar SDHA expression (Extended Data Fig. 7a) and succinate levels (Extended Data Fig. 7b) as WT B6 mice. However, following BMT, allogeneic *Irg1*$^{-/-}$ mice demonstrated reduced succinate levels (Extended Data Fig. 7c) with greater SDHA level, reduced clinical and intestine severity from GVHD (Extended Data Fig. 7e, f) than WT recipients.

Next, to directly assess and confirm whether reduction of SDHA in IECs made them more permissive to T cell mediated damage, we harvested IECs of WT B6, Sdha$^{\Delta/IEC}$ and *Irg1*$^{-/-}$mice and utilized them as direct targets of allo-primed T cells in CTL assay. IECs of Sdha$^{\Delta/IEC}$ showed higher levels of cell death when compared to IECs of WTB6. By contrast, *Irg1*$^{-/-}$ IECs showed less cell death than IECs from WT B6 (Extended Data Fig. 7g). We also used CRISPR-Cas9 mediated IRG1 KO PCECs as target cells for CTL assay. *Irg1* gene expression of IRG1 KO PCECs was decreased when compared to control PCECs (Extended Data Fig. 7h) and demonstrated reduced cell death when utilized as targets of in allogeneic CTL assay (Extended Data Fig. 7i, Supplementary Fig. 1c).

We next assessed whether short chain fatty acid butyrate that mitigated GVHD severity[18 19], ameliorated the metabolic defect of reduced SDHA in allo-IECs. Allo-animals treated with butyrate showed greater preservation of SDHA (Extended Data Fig. 7j) and reduced succinate accumulation (Extended Data Fig. 7k) when compared to the control allo-recipients. We hypothesized that the preservation of SDHA by butyrate might be related to transcriptional upregulation of SDHA by promoting histone acetylation. Chromatin immunoprecipitation (ChIP) of the IECs isolated from naïve mice and treated with non-

cytotoxic doses of butyrate demonstrated greater histone (H4) acetylation at the promoters of both *Sdha* and *Sdhab* genes when compared to vehicle treated compared with control treated cells (Extended Data Fig. 7l).

Mechanism of T cell mediated reduction of SDHA

To determine mechanism of reduction in SDHA, we performed transcriptomics of IECs harvested from syngeneic and allogeneic recipients 7 days after HCT and analyzed for the expression of OXPHOS genes (see Methods). We found no significant differences between syngeneic mice and allogeneic mice (Extended Data Fig. 8a, b). Furthermore, there was no significant difference in expression of mitochondrial complex II subunits, including SDHA, SDHB and SDHC between the groups (Extended Data Fig. 8c). These data suggested that the reduction in SDHA protein levels in the IECs from allo-recipients may likely be from post-transcriptional processes.

We next analyzed whether the reduction of SDHA in IECs was dependent on direct contact with T cells. The PCECs targets were incubated with T cells primed with syngeneic or allogeneic stimulators in a transwell assay. PCECs cultured with primed syngeneic T cells, as expected, did not show any increase in cell death regardless of contact. By contrast, only the PCECs that were in direct contact with allo-primed T cells, showed greater cell death when compared to those separated by transwell membrane from the allo-primed T cells (Fig. 7a). Importantly when the PCEC targets were isolated and stained with SDHA from these transwell experiments after 4 hours of culture, only the PCECs that were in direct contact with allo-primed T cells showed reduction in SDHA (Fig. 7b). These data demonstrated that reduction of SDHA in the IEC targets required direct contact by T cells primed against allo-antigen and that soluble mediators such as inflammatory cytokines were not the likely cause for reduction in SDHA levels in the IEC targets.

Correlation of loss of SDHA in humans

We next determined whether the loss of SDHA has any human, clinical relevance. To this end we obtained intestinal biopsy samples from 31 patients that underwent allogeneic HCT and received similar immunoprophylaxis and were clinically suspected of lower GI GVHD. They all then underwent GI biopsy for diagnostic confirmation. In about half of these patients, biopsy confirmed the clinical diagnosis and in the other half, the biopsy was read as negative for GI GVHD. These 31 samples were stained and quantified for SDHA expression and analyzed in a manner blinded to the clinical and histopathological diagnosis. SDHA expression was dramatically reduced in the colonic biopsy samples from patients that were histopathologically confirmed as GI GVHD (Fig. 7c, Extended Data Fig. 9). The SDHA fluorescence intensity levels were statistically significant between GVHD and non-GVHD samples (Fig. 7d).

DISCUSSION

Here we demonstrate a defect in mitochondrial complex II of the IECs that is common and exclusive for only T cell mediated diseases of the intestinal tract. We show that the IECs accumulate succinate as a consequence of reduction in their mitochondrial

complex II component, SDHA. This reduction in SDHA caused an enhanced sensitivity of the IECs to T cell mediated cytotoxicity, thus serving as an IEC intrinsic metabolic checkpoint that regulated disease severity independent of direct effects of immune cells. The inhibition of SDHA in IECs altered their bioenergetics, decreased OXPHOS without a compensatory increase in glycolysis, which led to reduced O2 utilization and enhanced ROS production. Utilizing combination of metabolic, chemical and genetic loss and gain of function approaches we demonstrate that SDHA reduction in IECs is a critical target tissue intrinsic pathway for T-cell mediated intestinal diseases such as alloimmune GI GVHD, autoimmune IBD, and iatrogenic CTLA-4Ig ICB mediated colitis. We further validated the observation in human samples of GI GVHD. These data identify tissue intrinsic SDHA as novel target to mitigate multiple T cell mediated intestinal immunopathologies[20]. T cell dependent contact was required for reduction of SDHA, but the specific, and the critical T cell contact dependent pathways that mediate SDHA reduction will need to be determined.

At homeostasis, IECs efficiently utilize β-oxidation via SCFAs, especially butyrate [21]. However, in the context of T cell colitis, IECs show a loss of their major energy pathway, TCA cycle, without a compensatory change to glycolysis, leading to a metabolic shutdown, which likely contributes to their greater susceptibility to cell death. Furthermore, MFA demonstrated that neither palmitate, glucose, nor glutamine demonstrating that mitochondrial complex II, SDHA and not enhanced anaplerosis or beta-oxidation caused accumulation of succinate in allo-IECs. This defect was however, at least in part, corrected by exogenous supplementation of butyrate, likely by increasing the expression of *Sdha* gene.

Succinate accumulation in IECs caused by SDHA reduction, is likely an early event, that enhances the permissiveness of IECs to T cell mediated damage and is distinct from other mitochondrial damage inducing insults[9 10 22]. However, decreased NADH production by insufficient TCA cycle, a substrate for complex I reaction the starting point of ETC, could also secondarily contribute to the metabolic shutdown in the IECs. Because complex II is a direct ROS generator, disruption of its activity by loss of function of SDHB and perhaps other components may also affect ROS levels affecting their ability to tolerate stress[23] such as for example, chemotherapy [24]. Our data suggest that the accumulated succinate in IECs may however act in an autocrine manner and enhance HIF1α dependent pathways, but not in paracrine manner because of absence of detectable level of SUCNR1 on IECs. The loss of normal intestinal tissue hypoxic niche in the context of allo-HCT suggest that O_2 changes are unlikely the cause for HIF1α expression.. The loss of physiologic hypoxia is likely from the lack of O_2 utilization by the IECs from the reduction in OXPHOS caused by loss of SDHA. It is tempting to speculate that this initial metabolic aberration in host IECs leads to dysbiosis observed in GVHD and IBD model systems. Nonetheless, the functional relevance of IEC intrinsic increase in succinate, HIF1α and the loss of hypoxia on IEC biology will need to be addressed in future studies.

Our data have several implications and raise interesting questions. First, the exact mechanisms remain to be understood and its value as potential clinical diagnostic or prognostic biomarker for GI damage from GVHD, IBD or ICB colitis will need to be validated in larger studies.

Second, the specific SDHA abnormality was neither observed in other known GVHD target organs, namely liver and skin(which are also caused by alloreactive T cells nor in non-T cell mediated damage of IECs. This suggests that the dominant metabolic pathways and their alterations in IECs may be distinct from other T cell target tissues. It is therefore tempting to speculate that distinct target tissues may be uniquely susceptible to T cell mediated cell death, depending on their preferred, intrinsic metabolic pathways. Conversely, the lack of increase in disease severity from reduction of SDHA in IECs in non-T cell mediated intestinal pathologies suggests that the lack of tissue tolerance to T cell is not due to a global loss of fitness.

Previous studies have demonstrated that granzyme B targets mitochondrial complexes and several other substrates in mammalian cells, bacteria and parasites[6, 25, 26, 27]. SDHA has been shown to be targeted by granzyme B in vitro studies in mammalian non-IEC cells, although the functional relevance was not explored [21]. Our data also showed reduction in SDHA and a modest reduction in complex III similar to aforementioned studies. Furthermore, our EM studies showed profound changes in the overall structure of mitochondria in allo-IEC besides showing reduction in SDHA. Given T cell contact dependence observed in our studies, it remains to be determined whether IEC mitochondrial complex changes are dependent on T-cell perforin-granzyme pathway and whether the mitochondrial structure are causally related to SDHA reduction in IECs. It is also formally possible that thechangesin other complexes subsequent to disruption of SDHA, may collectively contribute to the observed severity of damage. Finally, permissiveness to cell death caused by T cell dependent regulation of SDHA in IECs is germane to apoptosis and/ or to also other mitochondrial dependent cell death pathways such as pyroptosis mediated by gasdermin proteins [28,29,30] will need to be explored. . Our studies utilized $CD326^{+}$ enterocytes, but the intestinal tract has several subtypes and in distinct phases of differentiation, such as ISCs, Paneth cells, tuft cells, Goblet cells etc. The dominant metabolic pathways, bioenergetics for many of these cell subsets is distinct or remain to be understood and therefore, whether the reduction in SDHA and its functional consequences are similar in intestinal cellular subsets in the context of T cell mediated immune-pathology need to be understood.

Our data align with the notion that factors that promote tissue tolerance in infectious diseases may also extend to non-infectious T cell mediated colitis[31], although the mechanisms may differ. They demonstrate for the first time that target cell autonomous pathway (SDHA) is critical for non-infectious tissue tolerance, supporting the concept that optimal therapy for immune mediated diseases may need approaches that promote immune tolerance and tissue tolerance. Specifically our data suggest that that either increasing SDHA expression and/or reducing its degradation in IECs may alleviate T cell mediated colitis. Conversely, inhibiting SDHA in T cell targets may have therapeutic implications for enhancing T cell dependent immunotherapies. For example, it is possible that inhibiting SDHA in cancers where the tumor cells are dependent on OXPHOS may enhance their susceptibility to graft versus leukemia or ICB mediated cancer immunotherapy.

In summary we identify a novel IEC intrinsic metabolic checkpoint that regulates their sensitivity to T cell mediated cytotoxicity and identify the component of mitochondrial

complex II, SDHA, as a potential novel therapeutic target to regulate alloimmune, autoimmune and iatrogenic T cell mediated colitis.

Methods

Mice:

C57BL/6 (WT B6, H-2K^{b}, CD45.2), B6 Ly5.2 (H-2K^{b}, CD45.1), *B6.129S7-Rag1^{tm1Mom}/J*(*Rag-1$^{-/-}$*), *Sdhaf1$^{-/-}$*, *B6.Cg-Tg(ACTFLPe)9205Dym/J*, *B6.Cg-Tg(Vil-cre)1000Gum/J* mice, C3H.SW (H-2K^{b}, CD229.1), and C57BL/6N-Acod1em1(IMPC)J/J (*Irg1$^{-/-}$*) mice were purchased from the Jackson Laboratory (Bar Harbor, ME, USA). BALB/c (H-2K^{d}) and BDF1 (H-2K$^{b/d}$) mice were purchased from Charles River Laboratories. C57BL/6N-*Sdha$^{tm2a(KOMP)Wtsi}$* mice were obtained from Knock Out Mouse Project (KOMP) repository, University of California, Davis and bred to *ACTFLPe* mice to excise the *FRT*-flanked region (Extended Data Figure 6g). Then *Sdha$^{fl/fl}$* mice were bred to *Vil1-Cre* mice to create *Vil1-Cre Sdha$^{fl/fl}$* (*Sdha$^{\Delta/IEC}$*) mice. 8–12 weeks old female mice used for experiments. All mice were kept under specific pathogen-free (SPF) conditions and cared for according to regulations reviewed and approved by the University of Michigan Committee on the Use and Care of Animals (PRO00009494), which are based on the University of Michigan Laboratory Animal Medicine guidelines

Cell culture:

C57BL/6 primary colonic epithelial cells (PCEC, C57–6047, Cell Biologics) were cultured in Complete Epithelial Cell Medium (#M6621, Cell Biologics). Cells were routinely tested for mycoplasma contamination using MycoAlert (#LT07-318, Lonza). Cells were incubated with 4-Octyl itaconate (#SML2338, 0.1mM, Sigma-Aldrich). IC-21 cells (#TIB-186, ATCC) were cultured with lipopolysaccharides (LPS, #L4005, 100ng/ml, Sigma-Aldrich) for 12hours.

Hematopoietic cell transplantation:

Splenic T cells from donors were enriched, and T-cell-depleted BM (TCD-BM) was depleted of T cells by autoMACS (Miltenyi Biotec) utilizing CD90.2 microbeads (#130-121-278, Miltenyi Biotec). The details of HCT model were described in Supplementary table. Animals received vehicle or dimethyl malonate (DMM, #136441, 0.5g or 5g kg^{-1}, Sigma-Aldrich), dimethyl itaconate (DI, #09533, 0.25g or 2.5g kg^{-1}, Sigma-Aldrich), atpenin A5 (#11898, 0.9 μg or 9μg kg^{-1}, Cayman Chemical) or succinic acid (#S3674, 0.4g or 1.725g kg^{-1}, Sigma-Aldrich), according to manufacturer's instructions by flexible 20-gauge, 1.5-in. intra-gastric gavage needle every other day from day 0. The mice were randomly assigned to syngeneic, allogeneic or treatment groups in each experiment.

Systemic and histopathological analysis of GVHD:

Survival after HCT was monitored daily and assessed the degree of clinical GVHD weekly, as described previously [32]. Histopathological analysis of the liver, gastrointestinal (GI) tract, and lung, which are the primary GVHD target organs, was performed as described utilizing a semi-quantitative scoring system implemented in a blinded manner by a single pathologist (C.L.) [33]. After scoring, the codes were broken, and the data compiled.

Colitis models:

For the DSS colitis model, animals were provided with drinking water containing 2.5–3% DSS (#0216011010, MP Biomedicals) for 7 days. Mice were injected with 100μg of anti–CTLA-4 mAb (#BE0164, clone 9D9, Bio X Cell) or isotype control (#BE0086, MCP-11, Bio X Cell) twice (3 and 1 day before DSS administration). For the T-cell transfer induced colitis model, isolated splenic T cells from WT B6 mice were stained with DAPI (#422801, 1μM, Biolenged), APC-Cy7 anti-CD4 (#560246, GK1.5, 1:100, BD Biosciences, San Jose, CA), APC anti-CD25 (#101910, 3C7, 1:100, Biolegend), FITC anti-CD44 (#103006, IM7, 1:100, Biolegend) and PE anti-CD45RB (#103308, C363-16A, 1:100, Biolegend). $CD4^{+}CD25^{-}CD44^{-}CD45RB^{hi}$ cells were sorted with the MoFlo Astrios cell sorter (Beckman Coulter) and intraperitoneally injected into *Rag-1*$^{-/-}$ recipients.

Liquid chromatography mass spectrometry:

To quantitate tricarboxylic acid cycle metabolites in vivo, samples (colon, ileum and kidney) from mice 7 and 21days post HCT were harvested, homogenized, and snap-frozen in liquid N_2 for metabolomics analysis The details of the method were described in Supplementary Methods.

Acyl-carnitine quantitation:

Tissues were subjected to targeted metabolomics analysis by LC/MS for determination of acyl-carnitines as previously described[34]. Briefly, samples were homogenized in 25mM phosphate buffer (pH 4.9) and extracted with cold 2:1:1 isopropanol: acetonitrile: methanol. Known amounts of isotope-labeled carnitines were used as internal standards and analyzed for LC/ESI/MS/MS analysis, an Agilent 6410 triple quadruple MS system equipped with an Agilent 1200 LC system and electrospray ionization (ESI) source was utilized and were detected in the multiple reaction monitoring (MRM) mode and relative peak areas were obtained.

In vivo metabolic flux analysis:

Animals 7 and 21days post HCT were intragastrically gavaged with a bolus (2 g/kg) of either labeled ^{13}C-glucose (#CLM-1396-1, Cambridge Isotopes), non-labeled ^{12}C-glucose, or ^{13}C-potassium palmitate (#605751, 0.5 g/kg, Sigma-Aldrich) complexed 6:1 with fatty acid-free BSA (#A6003, Sigma-Aldrich) after 9h fasting. The small and large intestinal epithelial cells were then isolated 4 hours later and metabolites were extracted from cell lysates using a mixture of methanol, chloroform, and water (8:1:1) for metabolomics analysis. The details of the method were described in Supplementary Methods.

^{13}C-glucose or ^{13}C-glutamine (#CLM-1822, Cambridge Isotopes) tracing in vitro was performed using glucose-free DMEM (#A1443001, Thermo Fisher Scientific) supplemented with 1mM sodium pyruvate (#11360070, Thermo Fisher Scientific), 1% HEPES (#15630080, Thermo Fisher Scientific), 2% BSA (#126575, Sigma-Aldrich), 10uM Y-27632 (#Y0503, Sigma-Aldrich) and either 17.5mM ^{12}C or ^{13}C-glucose, and either 2mM ^{12}C or ^{13}C-glutamine. Isolated intestinal epithelial cells (IECs) from naïve, syngeneic and allogeneic animals 7 and 21 days post HCT were cultured for 2 hours in ^{12}C or ^{13}C glucose/glutamine labeling media. Intracellular metabolite fractions were prepared from cells that

were lysed with cold (−80°C) 80% methanol, then clarified by centrifugation. Metabolite pellets from intracellular fractions were normalized to the protein content of a parallel sample, and all samples were lyophilized via speed vac. Dried metabolite pellets from cells were re-suspended in 35 μL 50:50 MeOH: H_2O mixture for metabolomics analysis. The details of the method were described in Supplementary Methods. Metabolomics data have been deposited to the EMBL-EBI MetaboLights database (MTBLS3281).

Cell isolation:

Luminal contents from dissected colon and ileum were flushed with CMF buffer; Ca^{2+}/Mg^{2+} free HBSS (#14185052, Thermo Fisher Scientific) supplemented with 25mM sodium bicarbonate (#S6014, Sigma-Aldrich) and 2% FBS (#100–106, Gemini Bio Products, USA). Intestines were then minced into 5mm pieces, washed with CMF buffer four times, transferred to CMF with 5mM EDTA (#51201, Lonza), and incubated at 37 °C for 40 minutes (shaking tubes every 10 minutes). Supernatants containing IECs were then transferred through 100 μM cell filter followed by incubation on ice for 10 minutes to allow sedimentation. Supernatants were again transferred through a 75 μM cell filter. $CD326^+$ IECs were next purified with APC-anti-CD326 (G8.8, #118214, 1:200, Biolegend) and anti-APC magnetic microbeads (#130-090-855, Miltenyi Biotec).

Succinate dehydrogenase functional staining:

Specimens were dissected from naïve, syngeneic and allogeneic WT B6 mice at 7 and 21days post HCT. The tissues were rinsed in ice cold PBS and were then frozen in 2-methylbutane (#M32631, Sigma-Aldrich) and dry ice. Frozen sections (cut at 8μm thick) were directly placed in SDH solution; 48mM disodium succinate hexahydrate (#8201510100, Sigma-Aldrich), 0.75mM sodium azide (#S8032, Sigma-Aldrich), 0.5mM disodium EDTA (#324503, Sigma-Aldrich), 13mM sodium phosphate monobasic monohydrate (#S3522, Sigma-Aldrich), 87mM sodium phosphate dibasic heptahydrate (#S9390, Sigma-Aldrich), 998.9μM 1-methoxy-5-methylphenazinium methyl sulfate (M8640, Sigma-Aldrich), 1.5mM nitroblue tetrazolium (#484235, Sigma-Aldrich) at 37°C for 30 minutes and then the slides were rinsed in ddH_2O. After mounting the slides, images were obtained using Olympus BX51M (Olympus) and the SDH activity was quantified using Image J (National Institutes of Health).

Mitochondria Isolation:

Isolated IECs from syngeneic and allogeneic recipients in mitochondria isolation buffer (MIB) were disrupted using a glass homogenizer with 2–3 strokes. MIB was composed of 70mM sucrose (#S0389, Sigma-Aldrich), 210mM mannitol (#M9546, Sigma-Aldrich), 5mM HEPES, 1mM EGTA (#E0396, Sigma-Aldrich), 0.5% BSA, pH 7.2 and protease inhibitor cocktail (#78429, Sigma-Aldrich). Homogenate was centrifuged at 800 g for 10 min at 4°C. Following centrifugation, fat/lipid was carefully aspirated, and the remaining supernatant was decanted through 2 layers of cheesecloth to a separate tube and centrifuged twice at 8000g for 15 min at 4°C. After removal of the light mitochondrial layer, the pellet was resuspended in MIB and centrifuged at 8500g for 10min. The final pellet was resuspended in a minimal volume of mitochondrial assay solution (MAS) and kept on ice. MAS comprises 70mM sucrose, 220mM mannitol, 10mM potassium monobasic

phosphate (#P5655, Sigma-Aldrich), 5mM magnesium chloride (#M8266, Sigma-Aldrich), 2mM HEPES, 1mM EGTA, 0.2% BSA, and protease inhibitor cocktail at the pH of 7.2. Total protein (mg/ml) was determined via Pierce BCA Protein Assay (#23225, Thermo Scientific).

Immunoblot analysis:

Isolated mitochondria or IECs were lysed in RIPA buffer (#89901, Thermo Scientific). Equal amounts of proteins were loaded on 4–12% SDS-PAGE gel (#NP0321, Thermo Scientific), electrophoresed and subsequently transferred to a PVDF membrane (#ISEQ85R, Sigma-Aldrich) using a Bio-Rad semi-dry transfer cell (20 V, 1 h). Blots were incubated with anti-SDHA (#ab14715, 2E3GC12FB2AE2, 0.1μg/ml, Abcam), Total OXPHOS rodent antibody cocktail (#ab110413, 1:250, Abcam), anti-ClpP (#ab124822, 1:1000, Abcam), Tom20 (#42406, D8T4N, 1:1000, Cell Signaling Technology), SUNCR1 (LS-B15693, 1:500, LSBio) and anti-β actin (#8226, mAbcam8226, 1:3000, Abcam) primary antibodies overnight at 4°C. Incubation with secondary anti-rabbit-HRP (#7074S, Cell Signaling Technology), anti-mouse-HRP (#sc-516102, Santa Cruz Biotechnology) was performed at room temperature for 1 hour. Bound antibody was detected using Super Signal ECL substrate (Thermo Scientific) and quantitated using ChemiDoc MP Imaging system (BioRad, Hercules). Densitometric analysis was performed using Image J.

BN-PAGE:

Isolated mitochondria was lysed in NativePAGE sample buffer (#BN2008, Thermo Scientific) containing 2% digitonin. 50ug of total protein was loaded on 3–12% NativePAGE gel (#BN1001, Thermo Scientific). Gels were stained by Colloidal Blue Staining Kit (#LC6025, Thermo Scientific). For the second dimension, SDS-PAGE, gel lanes from BN gels were placed onto top of a 4–12% NuPage 2D well (#NP0326, Thermo Scientific). After separation and blotting, membranes were probed with Total OXPHOS blue native antibody cocktail (#ab110412, 1:250, Abcam).

Fluorescent immunohistochemistry staining:

Sections were prepared as mentioned in the SDH functional staining method. The sections were fixed in 4% paraformaldehyde (#P6148, Sigma-Aldrich) for 30 minutes. Then, the sections were washed 3 times in PBS and permeabilized in PBS containing 0.3% Triton-X100 (#X100, Sigma-Aldrich) for 2 hours. Permeabilized sections were blocked for 2 hours (10% normal goat serum in PBS containing 0.15% Triton X-100) and incubated with primary antibodies overnight at 4°C. The following primary antibodies were used; anti-SDHA (#ab14715, 2E3GC12FB2AE2, 1:100, Abcam) and COX IV (#ab16056, 20E8C12, 1:200, Abcam), overnight at 4. Incubation with secondary Cy3 anti-mouse-IgG (#405309, Poly4053, 1:250, BioLegend) and Dy-Light488 anti-rabbit-IgG (#406404, Poly4064, 1:250, BioLegend) was performed at room temperature for 1 hour. Slides were mounted with coverslips using Prolong Gold with DAPI (#P36931, Thermo Scientific). For hypoxia staining, recipient mice were administered pimonidazole (PMDZ) from Hypoxyprobe, Inc. by intraperitoneal injection 30 min prior to sacrifice. Colon and ileum samples were paraffin-embedded and stained according to the manufacturer's instructions and counterstained with DAPI [35]. For human samples, formalin fixed paraffin embedded

specimens from patients were cut to a thickness of 5 μm. Heat-induced antigen retrieval was performed with 10 mM sodium citrate buffer followed by staining with primary antibodies. Slides were imaged using a Nikon A1confocal microscope (Nikon). SDH levels were quantified and measured in intensity from Cy3 positive epithelial cells using Image J. For primary mice colonic epithelial cells, cells were spun down and put on coverslips. After 10 minutes of incubation at 37°C, cells were fixed with 3% paraformaldehyde for 20minutes, quenched with 100mM Glycine (#G8998, Sigma-Aldrich) 3 times for 3 minutes and permeabilized in PBS containing 0.3% Triton-X100 for 1 minute. Then, the cells were blocked, stained with primary and secondary antibodies, and mounted.

Transmission Electron Microscopy and immunogold immunohistochemistry:

Colon and ileum were harvested, diced into 1mm cubes and fixed with 4% formaldehyde and 2.5% glutaraldehyde (#G5882, Sigma-Aldrich) in 0.1 M phosphate buffer (PB, pH 7.4) overnight. Next, the tissues were immersed in 0.2 M sucrose and 0.1 M PB, and then post-fixed in 1% osmium tetroxide (#75632, Sigma-Aldrich) in 0.1 M PB. Then, the tissue was dehydrated in ascending concentrations of ethanol, treated with propylene oxide, and embedded in Epon epoxy resin. Semi-thin sections were stained with toluidine blue for tissue identification. Regions of interest were selected, cut into ultra-thin section (70 nm thick) mounted on copper grids, and then stained with uranyl acetate and lead citrate. For immunogold immunohistochemistry, sections were blocked with blocking solution for goat gold conjugates (#905.002, AURION) for 2 hours and then incubated with anti-SDHA antibody (1:10) overnight at 4°C. After rinsing, sections were incubated with 10nm gold particle conjugated anti-mouse IgG (H&L) (#810.022, 1:50, AURION) for 2 hours at room temperature and then fixed with 2.5% glutaraldehyde for 10 min before staining with 4% uranyl acetate for 15 minutes. The samples were examined using a JEM-1400 electron microscope (JEOL) at 80 kV. Images were recorded digitally using a XR401 camera system operated with AMT software (ver. 701, Advanced Microscopy Techniques Corp). Gold particles in the mitochondria were quantified in a blinded manner by L.L. After quantification, the codes were broken, and the data were compiled.

MtDNA Copy Number Analysis:

Total DNA was extracted from isolated IECs using the DNeasy Blood & Tissue Kit (#69504, QIAGEN). PowerUP SYBR green master mix (#A25742, Applied Biosystems) and the following primers were used; 5’-CAAACACTTATTACAACCCAAGAACA-3’ and 5’-TCATATTATGGCTATGGGTCAGG-3’ (*ND1; NADH: ubiquinone oxidoreductase core subunit 1*); 5’-AATCTACCATCCTCCGTGAAACC-3’ and 5’-TCAGTTTAGCTACCCCCAAGTTTAA-3’ (*D-loop1; displacement loop1*); 5’-CCCTTCCCCATTTGGTCT-3’ and 5’-TGGTTTCACGGAGGATGG-3’ (*D-loop2*) [36]; 5’-TCCTCCGTGAAACCAACAA-3’ and 5’-AGCGAGAAGAGGGGCATA-3’ (*D-loop3*); 5’- GCTTTCCACTTCATCTTACCATTTA-3’ and 5’-TGTTGGGTTGTTTGATCCTG-3’ (*CytB: cytochrome B*); 5’-CACTGCCTGCCCAGTGA-3’ and 5’-ATACCGCGGCCGTTAAA-3’ (*16S*); 5’-AACGGATCCACAGCCGTA-3’ and 5’-AGTCCTCGGGCCATGATT-3’ (*ND4*); and 5’-GCTTAATTTGACTCAACACGGGA-3’ and 5’-AGCTATCAATCTGTCAATCCTGTC-3’ (*18S).* All primers were verified for the production of a single specific PCR product via melting curve analysis.

Succinate quantification:

Isolated IECs were collected, processed and analysed using the Succinate Assay Kit (#ab204718, Abcam) according to the manufacturer's protocol.

Seahorse analysis:

IECs were resuspended with complete seahorse XF assay medium (#103335-100, Aglient) with 17.5 mM glucose, 1 mM sodium pyruvate, 2 mM glutamine, 2 %BSA 10uM Y-27632 and 1% penicillin-streptomycin (#516106, Sigma-Aldrich) adjusted to pH 7.4 with or without NADH (#10107735001, 1mM, Sigma-Aldrich). Cells were plated at 8×10^4 cells per well in a Seahorse assay plate, pretreated with matrigel (#354262, Corning). Cells were equilibrated to 37 °C for 30 min before assay. Respiration profile was assessed as described previously[37]. Comprehensive measurement of respiratory activity in permeabilized cells was performed on IECs d21 after HCT[5]. Cells were resuspended with MAS buffer and were plated at 8×10^4 cells per well in a Seahorse assay plate, pretreated with matrigel. Respiration profile was assessed in 96XF instrument with Mitostress assay as indicated upon cell treatment with 5 μM FCCP, 500mM sodium pyruvate, 250mM malic acid (#M0875, Sigma-Aldrich), 500mM succinic acid (#S3674, Sigma-Aldrich), 0.5μM rotenone, 500mM duroquinol (#T0822, TCI), 100mM ADP (#A2754, Sigma-Aldrich), 5μg/mL saponine (#SAE0073, Sigma-Aldrich), 7.5μM oligomycin and 4μM antimycin A. Seahorse Wave Desktop Software (version 2.6.1.53) was used for data analysis.

ATP detection assay: Isolated mitochondria from IECs were incubated in MAS supplemented with 5mM ADP (#A2754, Sigma-Aldrich), 10mM succinic acid and 2μM rotenone on white walled 96-well plates (#3917, Corning) at 8×10^4 cells per well in triplicate for 2 hours. The ATP level was measured using the Cell Titer Glo 2.0 luminescence assay (#G9243, Promega, Madison, WI). Luminescence was measured for 500ms using a SpectraMax M3 Microplate reader (Molecular Devices).

Complex I enzyme activity assay:

Isolated mitochondria from IECs were loaded on 96-well plates at 5μg per well in triplicate. Enzyme activity was measured using the colorimetric Complex I Enzyme Activity Assay Kit (#ab109721, Abcam) following manufacturer's instructions.

NAD^+/Nicotinamide Adenine Dinucleotide Diaphorase Assay:

Total intracellular NAD (NADH + NAD^+) and nicotinamide adenine dinucleotide diaphorase (NADH) levels in IECs were measured using the NAD^+/NADH Quantification Kit (#K337-100, BioVision) following the manufacturer's recommendations. The NAD^+/NADH ratio was then calculated based on levels of NAD and NADH.

In vitro allogeneic cytotoxic T lymphocyte assay:

Splenic T cells from WT-B6 and BALB/c animals and irradiated (30Gy) red blood cell lysed splenocytes from WT-B6 mice were co-cultured in 5:2 ratio for 96 hours. $CD8^+$ T cells were purified with a $CD8^+$ T-cell isolation kit (#130-117-044, Miltenyi Biotec) and used as effector cells. PCECs were pre-treated with 5mM DMM, 0.5mM DI, 10nM

atpenin A5, or vehicle for 3 hours. 2×10^6 treated cells were incubated with 2 MBq of $Na_2{}^{51}CrO_4$ (#NEZ030001MC, PerkinElmer, Waltham, MA) for 2 hours at 37 °C in a 5% CO_2 atmosphere and were used as target cells. After washing, 4×10^3 labeled targets were resuspended and added to triplicate wells at varying effector-to-target ratios and then incubated for 4 h. Maximal and minimum release was determined by the addition of Triton-X or media alone to targets, respectively.

For the transwell assays, 2×10^5 labeled targets were placed on the bottom chamber and effector cells were on the bottom or on the 0.4uM transwell membrane for 12 hours at 37 °C in 5% CO_2. Cells were incubated in fresh cell culture medium or conditioned from supernatant from effector cells. After incubation, supernatants were transferred to a Lumaplate (#600633, PerkinElmer) and ^{51}Cr activity was determined using Top Count NXT (Hewlett Packard).

For CTL assay of IECs, 1×10^4 isolated IECs of colon from B6WT, *Sdha*$^{\Delta/IEC}$ and *Irg1*$^{-/-}$ animals were added to triplicate wells pretreated with matrigel at effector-to-target ratio (50:1) and then incubated for 2 h with recombinant mouse IFN-gamma protein (#485-MI, 10ng/ml, R&D Systems). 7-AAD positive cells of APC-CD326 positive, FITC-CD45.2 negative cells was determined by Attune NxT flow cytometer (Thermo Scientific) and analyzed using FlowJo v10.2 (FlowJo LLC).

Flow cytometry:

Cells were re-suspended in 2% BSA in PBS and stained with the following antibodies and reagents; FITC-anti-CD326 (G8.8, #118208, 1:200), APC-anti-CD326 (G8.8, #118214, 1:200), DAPI, CellROX Deep Red (#C10491, 500nM, Thermo Scientific), MitoSOX (#M36008, 5μM, Thermo Scientific), JC-1 (#M34152, 2μM, Thermo Scientific), 7-AAD (#420404, 1:100, BioLegend), Annexin V (#640947, 1:20, Biolegend), anti-CD16/CD32 antibody (BD Biosciences, 2.4G2), APC-anti-CD45.2 (#109814, 1:200, BioLegend), FITC-anti-CD45.2 Mouse Monoclonal Antibody (#109806, 1:200, Biolegend), Green CMFDA Dye (#C7025, 1μM, Invitrogen), Anti-SDHA antibody (ab14715, 1:1000, Abcam), Anti-SDHB antibody (ab178423, 1:1000, Abcam), DyLight™ 488 anti-rabbit IgG antibody (#406404, 1:200, Biolegend) and APC anti-mouse antibody (#405308, 1:200, Biolegend) according to manufacturer's protocol. Cells were run on Attune NxT flow cytometer and analyzed using FlowJo v10.2.

RNA isolation and RT-PCR:

Total RNA from single-cell suspensions was isolated using the RNeasy Kit (#74104, QIAGEN) and reverse transcribed into cDNA using the High Capacity cDNA Reverse Transcription Kit (#4374966, Applied Biosystems). The following primers and PowerUP SYBR green polymerase were used to detect the following transcripts: 5′-ACATGCAGAAGTCGATGCAG-3′ and 5′- CATTCCCCTGTCGAATGTCT-3′ (Sdha); 5′-GCAACATGATGCTCAAGTCTG-3′ and 5′-TGCTCCTCCGAATGATACCA-3′ (Irg1); 5′-TGACCTCAACTACATGGTCTACA-3′ and 5′-CTTCCCATTCTCGGCCTTG-3′ (Gapdh). All reactions were performed according to manufacturer's instructions. All primers were verified for the production of a single specific PCR product via melting curve analysis.

Chromatin immunoprecipitation:

Isolated IECs on gelatin-coated (#6950, Cell Biologics) cell culture dishes (100 mm) treated them with 1 mM sodium butyrate overnight. We collected the cells and used them for ChIP analysis using SimpleChIP Plus Sonication Chromatin IP kit (#56383, Cell Signaling Technology) according to the manufacturer's instructions. The details of the method were described in Supplementary Methods.

Transcriptome analysis of colonic epithelial cells:

C57BL/6 mice received HCT (BALB/c or C57BL/6 → C57BL/6). IECs of colon from recipients were isolated from recipient mice at 7days after HCT and processed for RNA isolation. Total RNA from IECs was extracted using the RNeasy Kit (#74104, QIAGEN). Library preparations and sequencing reactions were conducted at GENEWIZ, LLC.. The details of the method were described in Supplementary Methods. All original data were deposited in the NCBI's GEO database (GSE158259).

CRISPR/Cas9-mediated knock-out in PCEC:

Control nontargeting crRNA (Integrated DNA Technologies) or IRG1-targeting crRNA (TGGTCGACCCCAAACAGTGC, CTGCTGCTGGCGTTCAACGT, GCTATTGCTGTTTCCCACGC) were complexed with tracrRNA (#1075928, IDT) at equimolar concentrations and annealed at 95°C for 5 minutes. crRNA-tracrRNA duplexes were complexed with Cas9 protein (#A36499, Invitorgen) at room temperature for 10 minutes. PCECs were resuspended in primary cell nucleofector solution (#V4XP-3032, Lonza) and mixed with Cas9/RNPs for 2 minutes at room temperature. Combined samples were transferred to a nucleofection cuvette, and electroporated on a Lonza 4D Nucleofector. KO efficiency was confirmed by qRT-PCR. Control and IRG1 KO PCECs were used as target cells for CTL assay.

Human patients and Data:

Colonic biopsy samples embedded in paraffin with deidentified and blinded patient data diagnosed as GVHD or non-GVHD from the University of Michigan Department of Pathology was provided without any information. All participants were provided written informed consents. All protocols and procedures for the human studies (HUM00043287; IRB 2001–0234) were approved by the Institutional Review Boards of the University of Michigan Medical School.

Statistical analysis:

All statistical analysis was performed using Graph Pad Prism (v8.0.0, Graph Pad Software Inc) and Excel2016 (version2105) to do the graph figures and statistics. P values <0.05 were considered as significant: P values >0.05 were considered as non-significant. All sample sizes and statistical tests used are detailed in each figure legend.

Extended Data

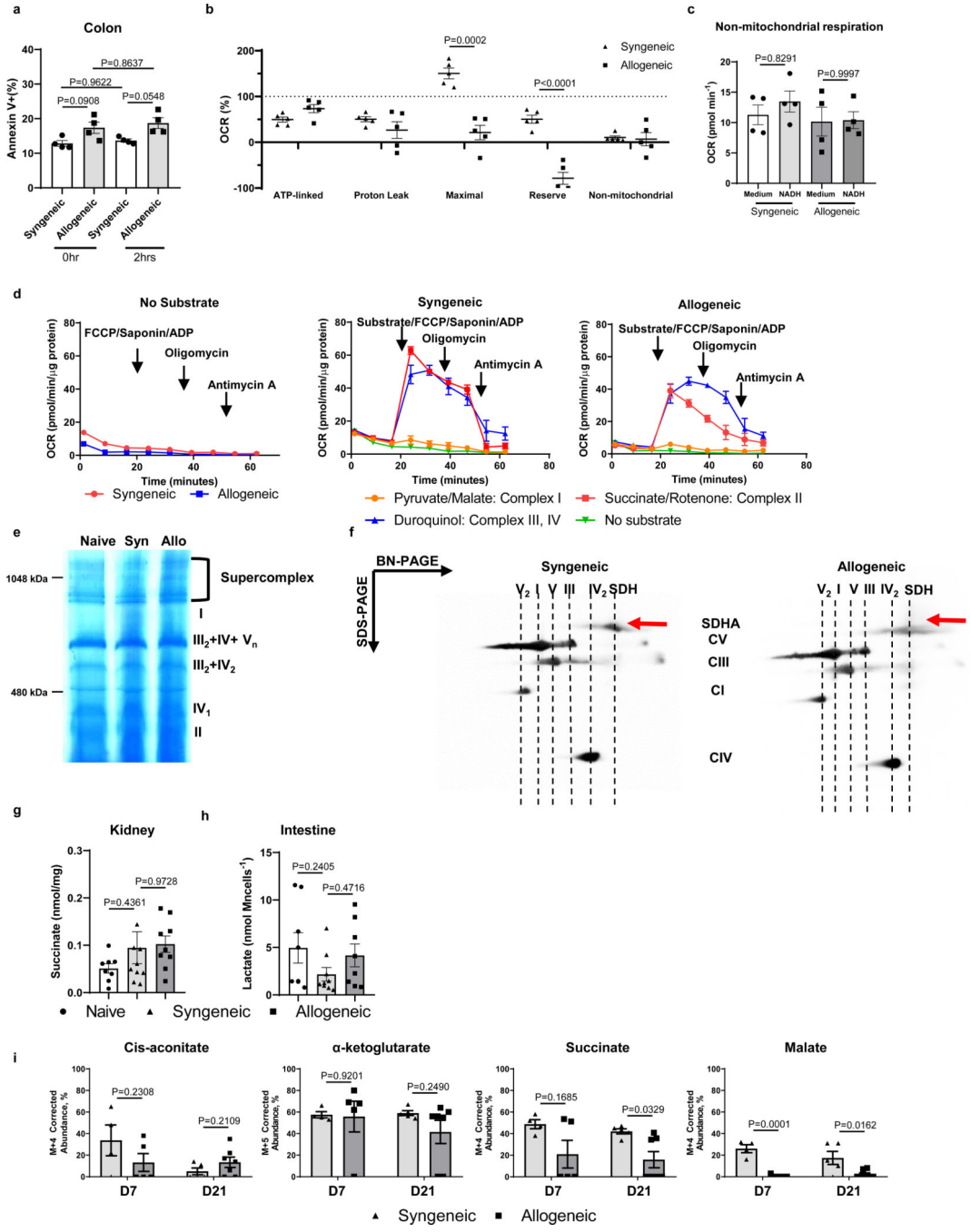

Extended Data Figure. 1: Mitochondrial respiration and metabolic pathway in IECs after allo-HCT.

C57BL/6 animals received HCT (BALB/c or C57BL/6→C57BL/6). (**a**) IECs of colon 7days post-HCT were isolated and incubated with medium. Cell death (AnnexinV+) was determined before incubation and after 2hours incubation (n=4). (**b**) Mitochondrial bioenergetic profile was determined as previously described [37]. % OCR change of several parameters in mitochondrial and non-mitochondrial cellular respiration normalized from

basal respiration in IECs of colon 21days post-HCT (n=5). (**c**) Non-mitochondrial OCR of IECs 21days post HCT with or without NADH (n=4). (**d**) Comprehensive measurement of respiratory activity in permeabilized IECs 21days post HCT. OCR of IECs without substrates of complexes (left). The combined OCR of syngeneic (middle) and allogeneic IECs (right) treated with each substrate (n=3). (**e**) Representative BN-PAGE image of mitochondria from IECs 21days post HCT showing abundant mitochondrial protein complexes (n=4). (**f**) Representative 2D-PAGE images of mitochondria from IECs on day21 post HCT showing reduced expression of SDHA protein (arrow, n=4). (**g-h**) Succinate levels in kidney (**g**, Naïve: n= 8, Syngeneic(Syn): n=10, Allogeneic (Allo): n=10) and lactate levels (**h**, Naïve: n= 8, Syn: n=9, Allo: n=8) in IECs from syngeneic and allogeneic recipients d21 post HCT with colorimetric methods. (**i**) Abundance from uniformly ^{13}C-glutamine of cis-aconitate, α-ketoglutarate, succinate, and malate after 4 h incubation in syngeneic or allogeneic isolated IECs 7 and 21days post HCT (D7 Syn: n=4, Allo: n=5, D21 Syn: n=5, Allo: n=7). All data are from biologically independent animals. Representative plots and a graph summarizing the results of at least two independent experiments are shown. One-way ANOVA analysis with Tukey post hoc test (**a**, **c, g, h**) or two-tailed unpaired t-test (**b**, **i**) were used to determine significance (mean ± s.e.m.).

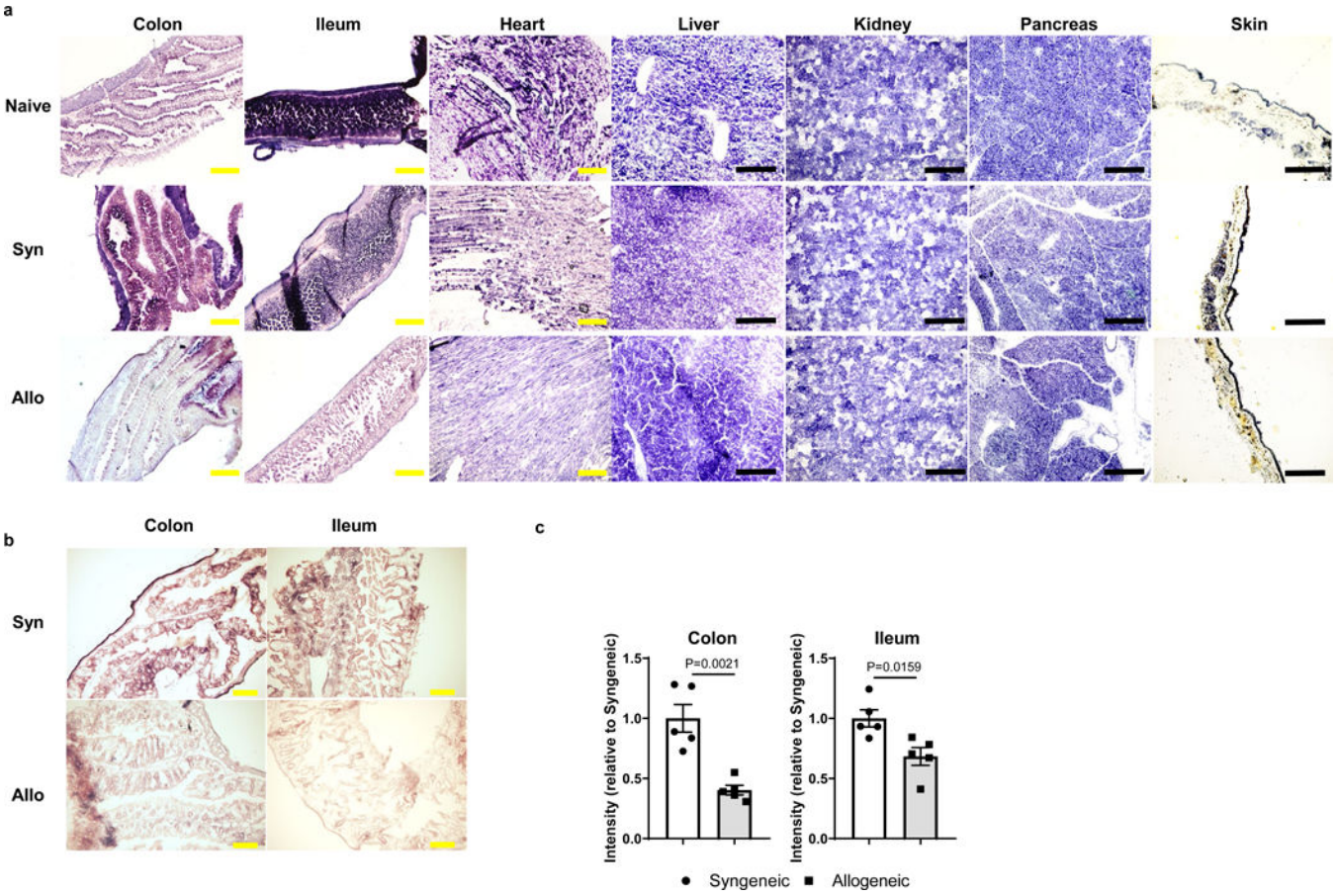

Extended Data Figure. 2: Specific reduction of SDHA activity in colon and ileum post allo-HCT.

C57BL/6 animals received 10 Gy total body irradiation and received 3×10^6 (BALB/c→C57BL/6) or 1×10^6 (C3H.SW→C57BL/6) T cells along with 5×10^6 TCD-BM cells from either syngeneic or allogeneic donors. (**a**) Representative images of SDH enzyme activity staining in GVHD target tissues (colon, ileum, liver and skin) and non-target tissues (heart, pancreas and kidney) from naive animals or recipients 21days post HCT (BALB/c→C57BL/6,). (b) Representative images of SDH enzyme activity staining in GVHD target tissues (colon, ileum) from recipients 21days post HCT (C3H.SW→C57BL/6). (**c**) Integrated intensity of SDH enzyme activity staining from colon and ileum 7days post HCT (BALB/c→C57BL/6, n=5 biologically independent animals). Representative plots and a graph summarizing the results of at least two independent experiments are shown. Scale bar (**a,b**): yellow=500μm, black=200 μm. All statistical analysis by two-tailed Mann-Whitney test (**c**) (mean ± s.e.m.).

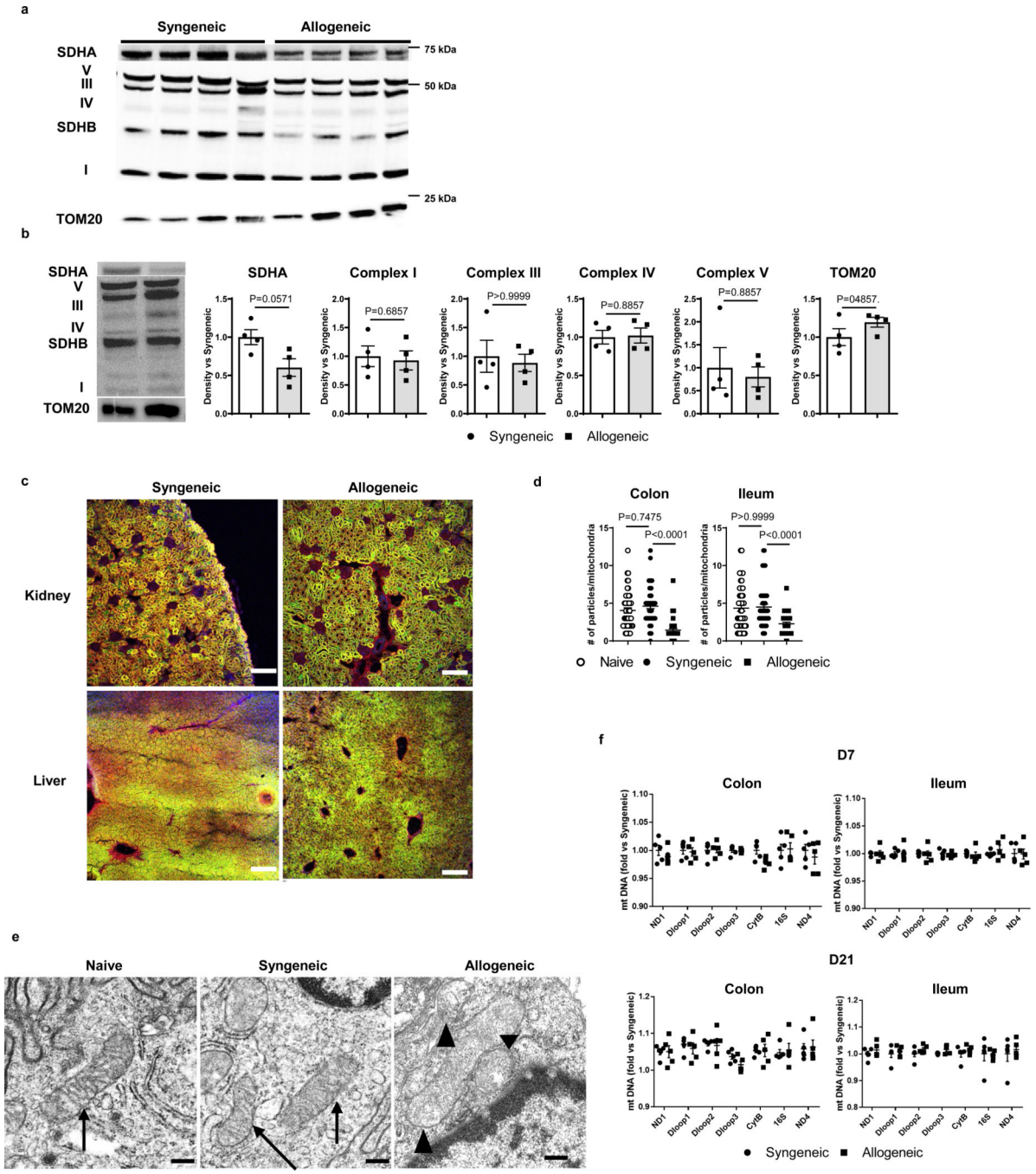

Extended Data Figure. 3: Morphological mitochondrial changes but not numbers in IECs post allo-HCT.

C57BL/6 animals received HCT (BALB/c or C57BL/6→C57BL/6). (**a**) Immunoblot of SDHA, complex V, III, IV, SDHB, I and TOM-20 in mitochondria from colonic IECs 21days post HCT (n=4). (**b**) Immunoblot and protein density quantification of SDHA, complex I, III, IV, V, SDHB, and TOM-20 in mitochondria from colonic IECs 7days post HCT (n=4). (**c**) Representative images of immunofluorescence staining of kidney and liver from recipients 21days post HCT (Complex IV=green, SDHA=red, DAPI=blue,

scale bar= 50 μm, n=5). (**d**) Numbers of gold particles per mitochondrial from colon and ileum of naïve animals or recipients 7days post HCT in transmission electron microscopy images with immune-gold staining of SDHA (total 50 mitochondria from 3 samples). (**e**) Representative images of transmission electron microscopy in mitochondria of colon from naive or recipients 21days post HCT (scale bar =200nm). Arrow indicates normal cristae and arrowhead indicates abnormal cristae (n=3). (**f**) Mitochondria DNA relative copy numbers of colon and ileum from syngeneic and allogeneic recipients 7 and 21days post HCT (n=5). All data are from biologically independent animals. Representative plots and a graph summarizing the results of at least two independent experiments are shown. All statistical analysis by two-tailed Mann-Whitney test (**b**) or one-way ANOVA analysis with Tukey post hoc test (**d**) (mean ± s.e.m.).

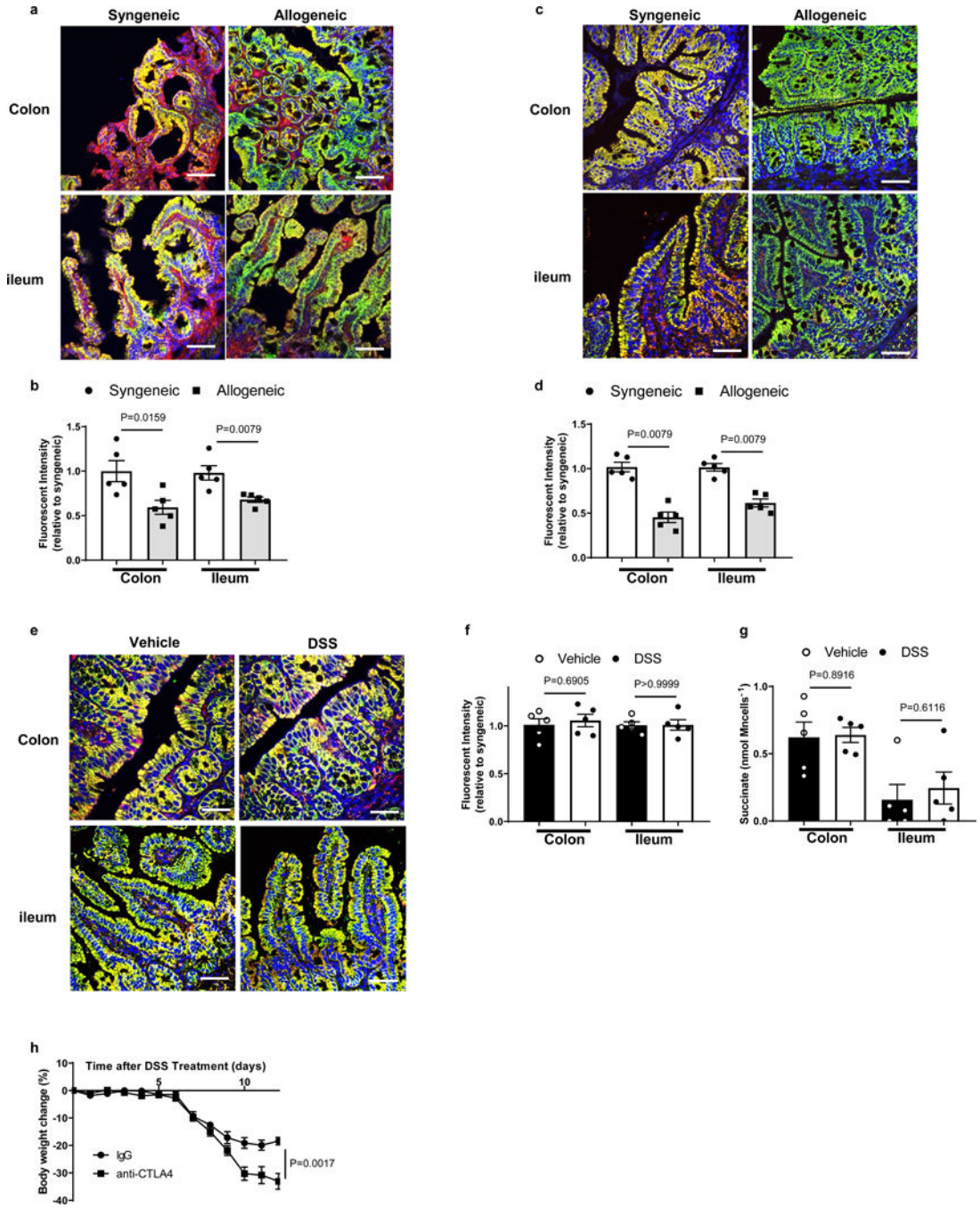

Extended Data Figure. 4: Conditioning regimen does not affect SDHA expression in IECs.

(**a-b**) C57BL/6 mice received 10 Gy total body irradiation followed by 1×10^6 T cells along with 5×10^6 TCD-BM cells from either syngeneic C57BL/6 or allogeneic mHA-mismatched C3H.SW donors (n=5). (**a**) Representative images of immunofluorescence staining and (**b**) fluorescent intensity of SDHA in colon and ileum from recipients 28days post HCT are shown. (**c-d**) C57BL/6 mice received chemotherapy and received 1×10^7 T cells along with 1×10^7 TCD-BM cells from either syngeneic C57BL/6 or allogeneic BALB/c donors (n=5). (**c**) Representative images of immunofluorescence staining and (**d**) fluorescent intensity of

SDHA in colon and ileum from recipients 21days post HCT. (**e-g**) C57BL/6 mice were treated with 3% DSS or vehicle in drinking water for 7 days (n=5). (**e**) Representative images of immunofluorescence staining and (**f**) fluorescent intensity of SDHA in colon 12days after DSS treatment. (**g**) Succinate levels in isolated IECs from colon and ileum of mice treated with 3% DSS at day12. (**h**) C57BL/6 mice receiving isotype control IgG or anti-CTLA-4 antibody were treated with 3% DSS in drinking water for 7 days. Time course of body weight changes after DSS administration. All data are from biologically independent animals. Representative plots and a graph summarizing the results of at least two independent experiments are shown. Scale bar (**a, c, e**) =50μm. All statistical analysis by two-tailed Mann-Whitney test (**b, d, f**) or two-tailed unpaired t-test (**g, h**) (mean ± s.e.m.).

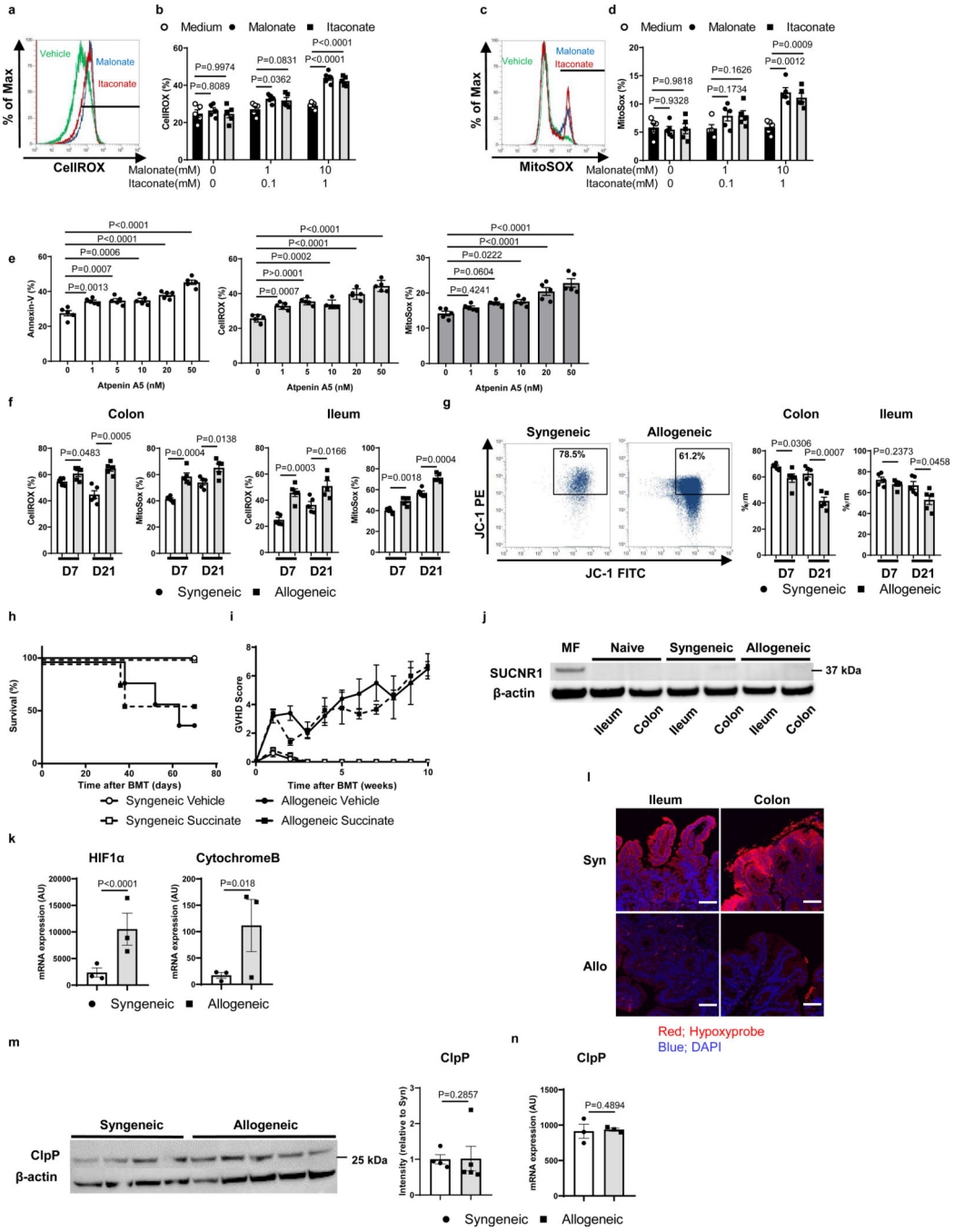

Extended Data Figure. 5: SDH inhibition causes ROS accumulation in IECs.

(**a-d)** PCECs were treated with DMSO, malonate or itaconate for 6 hours (n=5). Cytoplasmic ROS measured by CellROX staining. (**a**) Representative images and (**b**) CellROX positive cells are shown. Mitochondria ROS measured by MitoSOX staining. (**c**) Representative images and (**d**) MitoSOX positive cells are shown. (**e**) PCECs were treated with DMSO or atpeninA5 for 4hours. Cell death (left), CellROX (middle) and MitoSOX (right) levels were determined (n=5). (**f, g**) Colon and ileum IECs were isolated from HCT recipients (BALB/c→C57BL/6). CellROX, MitoSOX (**f**) and mitochondrial membrane

potential (ψm) (**g**) levels in (n=5). (**h, i**) HCT settings are described in (**f**). Recipients orally received succinate every other day from day0 post HCT. Survival (**h**) and GVHD severity (**i**) are shown (n=5). (**j**) Immunoblot of SUCNR1 in macrophage (MF, IC-21 cells) and IECs from BMT recipients 7days post HCT. Three independent experiments were performed. (**k**) Transcriptome analysis of IECs from recipients 7days post HCT. The mRNA expression of HIF1α and cytochromeB (n=3). (**l**) Representative images of Hypoxyprobe in colon and ileum from recipients 7days after HCT (scale bar= 50 μm). Four independent experiments were performed. **(m)** Immunoblot image and protein density of ClpP in IECs from recipients 21days post HCT (Syn: n=4, Allo n=5). (**n**) Transcriptome analysis of IECs from recipients 7days post HCT. The mRNA expression of ClpP (n=3). Data (**f, g, k, l, m, n**) are from biologically independent animals. Three independent experiments (**a-e**) were performed. All statistical analysis by one-way ANOVA analysis with Tukey post hoc test (**b, d, e**), two-tailed unpaired t-test (**f, g**), log-rank test (**h**) or two-tailed Mann-Whitney test (**m**) (mean ± s.e.m.). The p-values of the transcriptome analysis (**k, n**) obtained from DESeq-analysis.

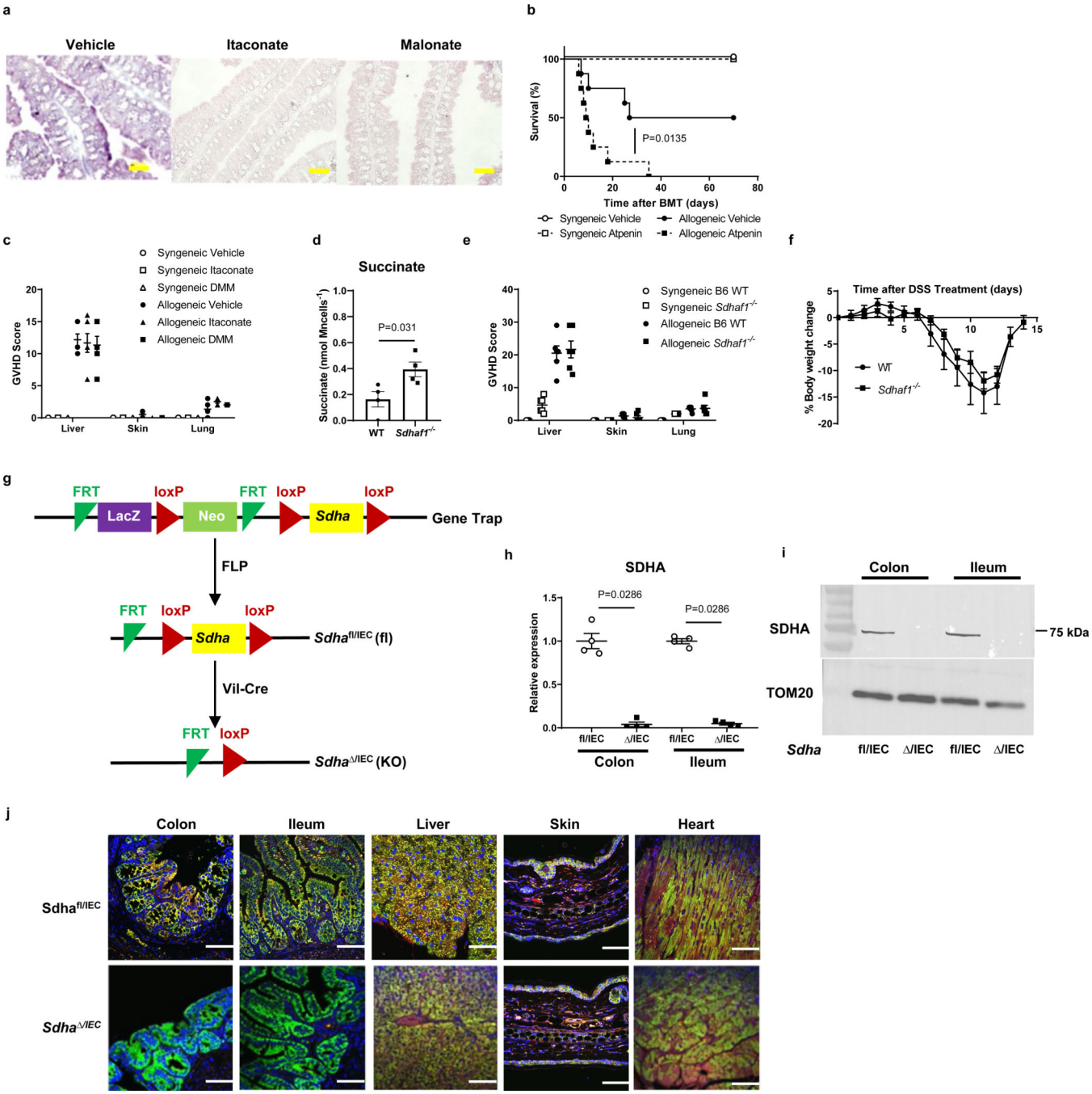

Extended Data Figure. 6: Chemical inhibition and genetic ablation of SDHA in IECs regulate the severity of GVHD.

(**a**) Representative images of SDH enzyme staining of colon from naive C57BL/6 12 hours after vehicle, malonate (5g kg^{-1}) or itaconate (2.5g kg^{-1}) treatment. (Scale bar 100μm, n=2). (**b-e**) C57BL/6 or *Sdhaf1*$^{-/-}$ animals received 10 Gy total body irradiation followed by 3×10^6 T cells along with 5×10^6 TCD-BM cells from either syngeneic C57BL/6 or allogeneic BALB/c donors. (**b**) Survival of C57BL/6 recipients treated with vehicle or atpeninA5 (9μg kg^{-1}) every other day post HCT (n=8). (**c**) C57BL/6 recipients treated

with vehicle, malonate (5g kg^{-1}) or itaconate (2.5g kg^{-1}) every other day post HCT. Pathological GVHD scores in liver, skin and lung 7days post HCT (n=6). (**d**) Succinate levels in isolated IECs from colon of naïve C57BL/6 mice and *Sdhaf1*$^{-/-}$ mice (n=4). (**e**) Pathological GVHD scores in liver, skin and lung 7days post HCT from C57BL/6 and *Sdhaf1*$^{-/-}$ recipients (n=6). (**f**) C57BL/6 and *Sdhaf1*$^{-/-}$ animals were treated with 2.5 % DSS in drinking water for 7 days. Time course of body weight changes after DSS administration (n=6). (**g**) Scheme illustrating the strategy used to generate *Sdha* floxed and excised alleles in IECs. (**h**) Expression of *Sdha* mRNA in CD326^{+} isolated IECs from six-week-old *Sdha*$^{\Delta/IEC}$ relative to *Sdha*$^{fl/IEC}$ mice (n = 4). *Sdha* expression was normalized to *Gapdh* expression. (**i**) Immunoblot of SDHA and TOM-20 in mitochondria of IECs from six-week-old *Sdha*$^{\Delta/IEC}$ and *Sdha*$^{fl/IEC}$ mice. (**j**) Representative images of immunofluorescence staining of colon, ileum, liver, skin and heart from six-week-old *Sdha*$^{\Delta/IEC}$ and *Sdha*$^{fl/IEC}$ mice (Complex IV=green, SDHA=red, DAPI=blue, scale bar=50μm, n=4). Data (**a-f, h**) are from biologically independent animals. All statistical analysis by log-rank test (**b**), Kruskal-Wallis analysis with Dunn's post hoc test (**c**), two-tailed unpaired t-test (**d**), or two-tailed Mann-Whitney test (**e, h**) (mean ± s.e.m.).

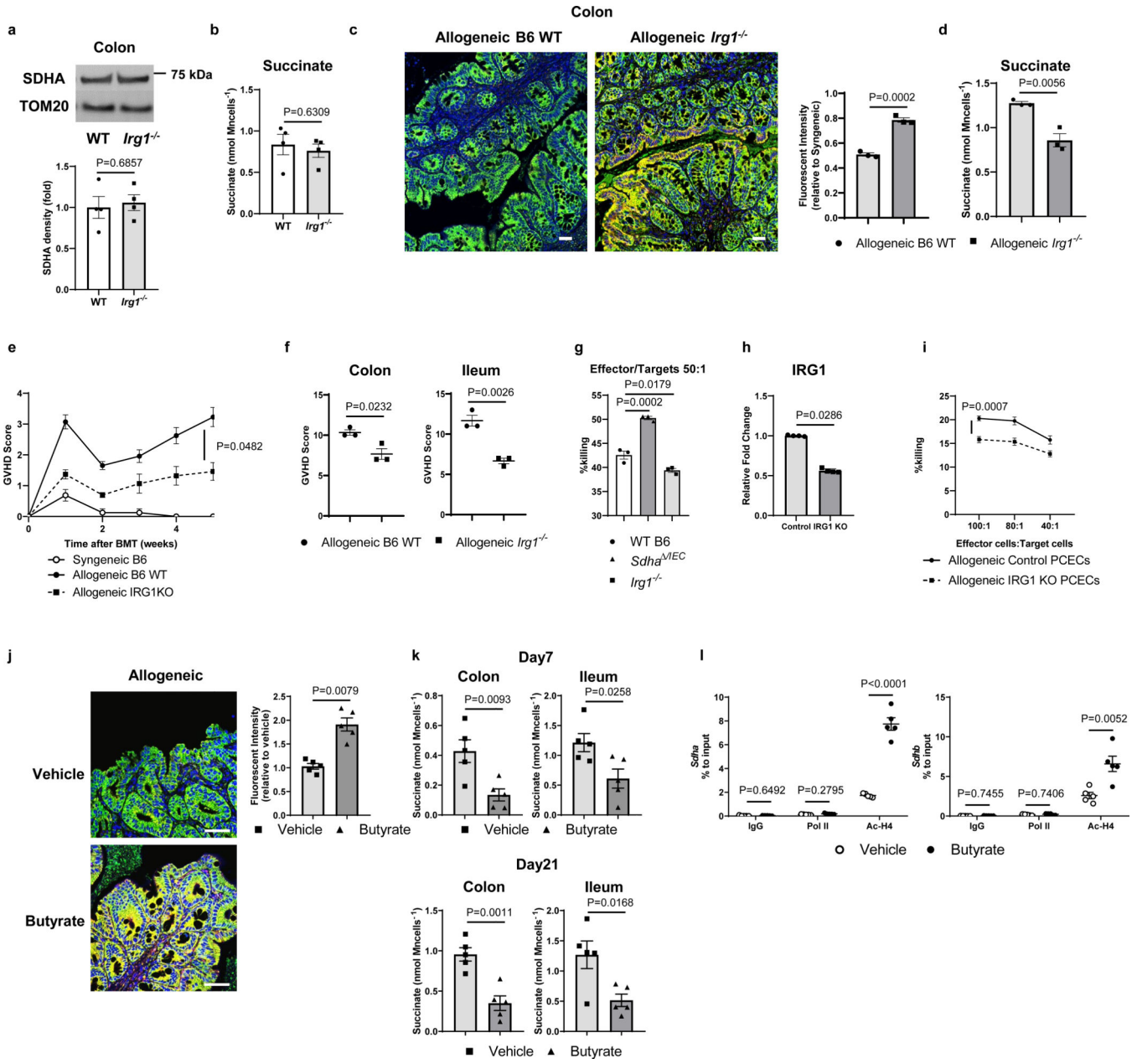

Extended Data Fig. 7: Increased SDHA levels reduce T cell mediated intestinal damage.

(**a, b**) Immunoblot and protein density quantification of SDHA (**a**) and succinate levels (**b**) in colonic IECs from naïve C57BL/6 and *Irg1*$^{-/-}$mice (n=4). (**c-f)** C57BL/6 animals *Irg1*$^{-/-}$ animals received HCT (BALB/c→C57BL/6 or *Irg1*$^{-/-}$) (**c**) Images (left) and fluorescent intensity (right) of immunofluorescence staining of colon on 21 days after post allo-HCT (Complex IV=green, SDHA=red, DAPI=blue, n=3). (**d**) Succinate levels in colon IECs at day21 post allo-HCT (n=3). Clinical GVHD severity (**e**) and pathological GVHD score (**f**) of ileum and colon after post HCT (Clinical GVHD severity, Syn C57BL/6: n=8, Allo C57BL/6 and *Irg1*$^{-/-}$: n=15, pathological GVHD score, n=3). (**g**) Colonic IECs from C57BL/6, *Sdha*$^{\Delta/IEC}$ and *Irg1*$^{-/-}$ were used as target cells for CTL assay (2hr co-culture with

effector T cells). Cell death was analyzed (n=3). (**h, i**) PCECs mediated by CRISPR-Cas9 targeting IRG1 were treated with LPS (100ng/ml)/ IFNγ(10ng/ml) for 6hr. (**h**) *Irg1* gene expression levels (normalized to *Gapdh* expression, n=4 cells examined over 3 independent experiments). (**i**) Control and IRG1 KO PCECs were used as target cells for CTL assay (7hr co-culture with effector T cells). Data are from 1 of 3 similar experiments) (**j, k)** C57BL/6 animals received HCT (BALB/c→C57BL/6) and treated with vehicle or butyrate. (**j**) Representative images (left) of immunofluorescence staining (Complex IV=green, SDHA=red, DAPI=blue) (left) and fluorescent intensity (right) of SDHA in colon on day21 post allo-HCT (n=5). (**k**) Succinate levels in IECs from colon and ileum on day7 (top) and day21 (bottom) post allo-HCT (n=5). (**l**) ChIP assay of 1mM butyrate-treated isolated colonic IECs from naïve C57BL/6 binding control IgG, pol II or acetylated histone H4 in the promoter regions of *Sdha* and *Sdhb* (n=5). Data (**a-d, f, g, j-l**) are from biologically independent animals. Scale bar (**c, j**) = 50 μm. All statistical analysis by two-tailed Mann-Whitney test (**a, h, j**), two-tailed unpaired t-test (**b, d, f, i, k, l**), Kruskal-Wallis analysis with Dunn's post hoc test (**e**) or ANOVA analysis with Tukey post hoc test (**g**) (mean ± s.e.m.).

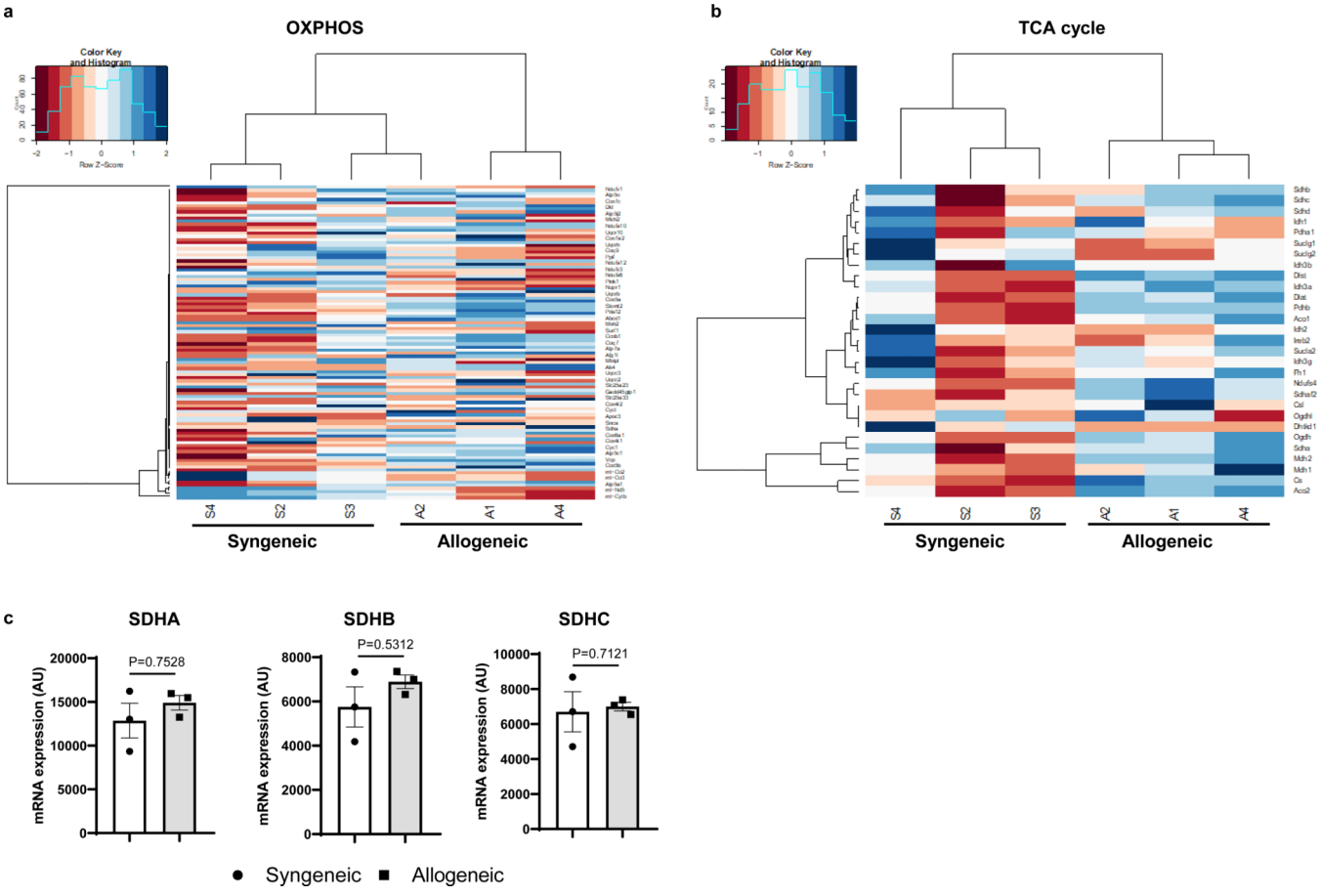

Extended Data Figure. 8: Transcriptome analysis of IECs after allo-HCT.

(**a-c**) C57BL/6 animals received 10 Gy total body irradiation followed by injection of 3×10^6 T cells along with 5×10^6 TCD-BM cells from either syngeneic C57BL/6 or allogeneic BALB/c donors. Transcriptome analysis of colonic IECs from syngeneic and allogeneic

recipients 7days post HCT. Heatmap of OXPHOS pathway gene (**a**) and TCA cycle related gene (**b**). (**c**) The mRNA expression of SDHA (left), SDHB (middle) and SDHC (right) in IECs from syngeneic and allogeneic recipients (n=3 biologically independent animals). The p-values of the transcriptome analysis (**c**) obtained from DESeq-analysis (mean ± s.e.m.).

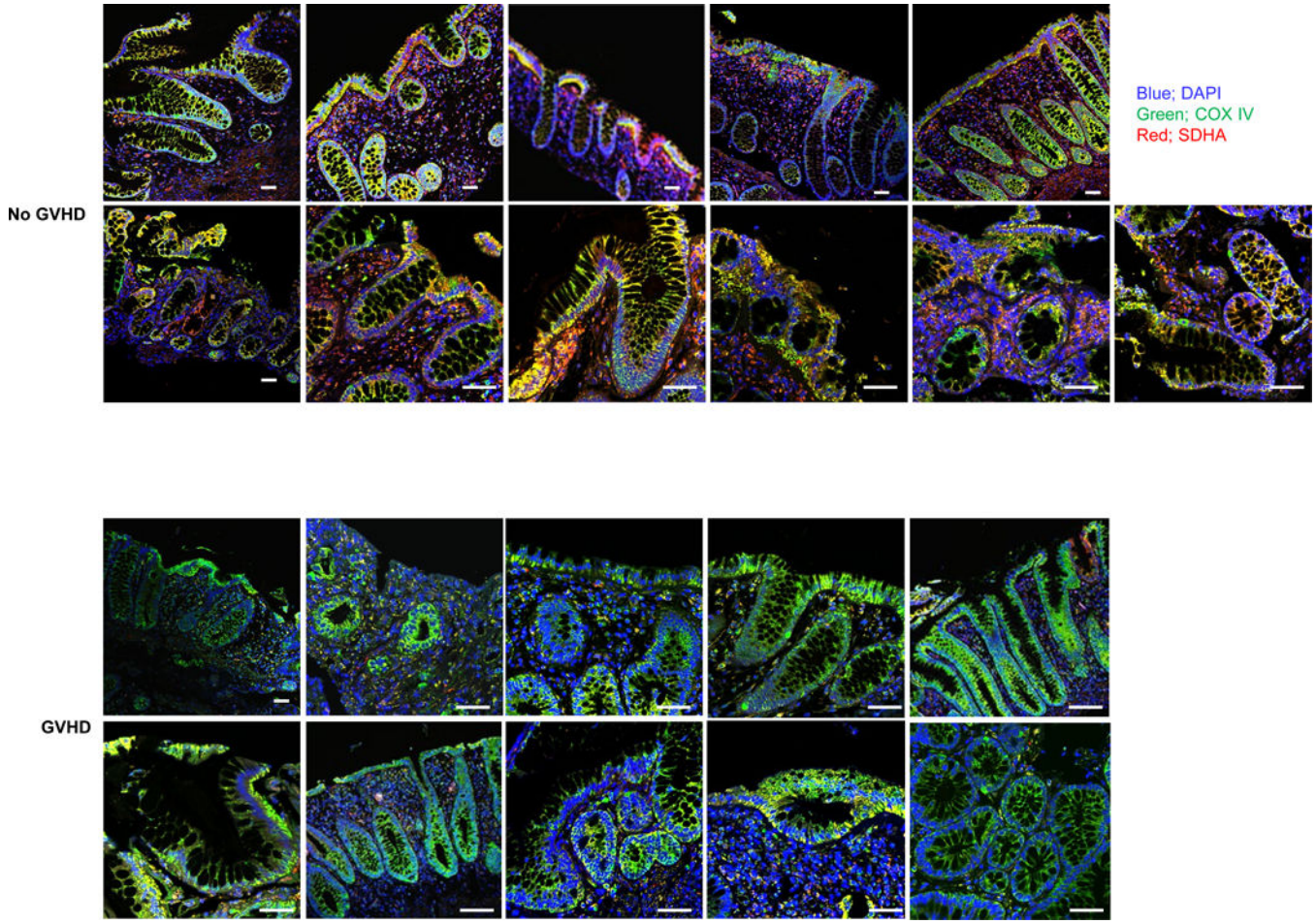

Extended Data Figure. 9: SDH expression in IECs from GVHD and non-GVHD patients.
Other representative images of immunofluorescence staining of colonic biopsy samples from patients suspected as having clinical GVHD after HCT not shown in Fig.7c (Complex IV=green, SDHA=red, DAPI=blue, scale bar= 50 μm). Two independent experiments are performed.

Supplementary Material

Refer to Web version on PubMed Central for supplementary material.

Acknowledgments:

This work was supported by the US National Institutes of Health grants HL090775, CA173878, CA203542, HL149633 (P.R.), K08HL130944 (A.V.M), DK081943, DK89503 (SP), JSPS Postdoctoral Fellowships for Research Abroad (H.F.), The YASUDA Medical Foundation Grants for Research Abroad (H.F.), JSPS KAKENHI Grant number JP20K22901, JP21H02904 (H.F.), The Kawasaki Foundation of Medical Science and Medical

Welfare (H.F.), The Ryobiteien Memorial Foundation (H.F.), The MSD Life Science Foundation Public Interest Incorporated Foundation (H.F.), The Okayama Medical Foundation (H.F.), The SENSHIN Medical Research Foundation (H.F.), The Kato Memorial Bioscience Foundation (H.F.) and The NOVARTIS Foundation (Japan) for the Promotion of Science (H.F.). We acknowledge use of the Microscopy & Image-analysis Laboratory (MIL) of the University of Michigan's Biomedical Research Core Facilities for the preparation of samples and images. Support for the MIL core is provided by the University of Michigan Rogel Cancer Center (NIH grant CA46592).

Data availability:

Transcriptome data were deposited in the NCBI's GEO database (GSE158259). Metabolomics data have been deposited to the EMBL-EBI MetaboLights database (DOI: 10.1093/nar/gkz1019, PMID:31691833) with the identifier MTBLS3281.

References;

1. Strober W, Fuss I. & Mannon P. The fundamental basis of inflammatory bowel disease. J Clin Invest 117, 514–521 (2007). [PubMed: 17332878]
2. Martins F. et al. Adverse effects of immune-checkpoint inhibitors: epidemiology, management and surveillance. Nat Rev Clin Oncol 16, 563–580 (2019). [PubMed: 31092901]
3. Ferrara JL, Levine JE, Reddy P. & Holler E. Graft-versus-host disease. Lancet 373, 1550–1561 (2009). [PubMed: 19282026]
4. Fan YY et al. A bioassay to measure energy metabolism in mouse colonic crypts, organoids, and sorted stem cells. Am J Physiol Gastrointest Liver Physiol 309, G1–9 (2015). [PubMed: 25977509]
5. Salabei JK, Gibb AA & Hill BG Comprehensive measurement of respiratory activity in permeabilized cells using extracellular flux analysis. Nat Protoc 9, 421–438 (2014). [PubMed: 24457333]
6. Jacquemin G. et al. Granzyme B-induced mitochondrial ROS are required for apoptosis. Cell Death Differ 22, 862–874 (2015). [PubMed: 25361078]
7. Wang F, Yin Q, Chen L. & Davis MM Bifidobacterium can mitigate intestinal immunopathology in the context of CTLA-4 blockade. Proc Natl Acad Sci U S A 115, 157–161 (2018). [PubMed: 29255057]
8. Perez-Ruiz E. et al. Prophylactic TNF blockade uncouples efficacy and toxicity in dual CTLA-4 and PD-1 immunotherapy. Nature 569, 428–432 (2019). [PubMed: 31043740]
9. Mills EL et al. Succinate Dehydrogenase Supports Metabolic Repurposing of Mitochondria to Drive Inflammatory Macrophages. Cell 167, 457–470.e413 (2016). [PubMed: 27667687]
10. Bailis W. et al. Distinct modes of mitochondrial metabolism uncouple T cell differentiation and function. Nature 571, 403–407 (2019). [PubMed: 31217581]
11. Tannahill GM et al. Succinate is an inflammatory signal that induces IL-1beta through HIF-1alpha. Nature 496, 238–242 (2013). [PubMed: 23535595]
12. Littlewood-Evans A. et al. GPR91 senses extracellular succinate released from inflammatory macrophages and exacerbates rheumatoid arthritis. Journal of Experimental Medicine 213, 1655–1662 (2016). [PubMed: 27481132]
13. Kuo CY, Chiu YC, Lee AY & Hwang TL Mitochondrial Lon protease controls ROS-dependent apoptosis in cardiomyocyte under hypoxia. Mitochondrion 23, 7–16 (2015). [PubMed: 25922169]
14. Ishizawa J. et al. Mitochondrial ClpP-Mediated Proteolysis Induces Selective Cancer Cell Lethality. Cancer Cell 35, 721–737 e729 (2019). [PubMed: 31056398]
15. Ghezzi D. et al. SDHAF1, encoding a LYR complex-II specific assembly factor, is mutated in SDH-defective infantile leukoencephalopathy. Nat Genet 41, 654–656 (2009). [PubMed: 19465911]
16. Na U. et al. The LYR factors SDHAF1 and SDHAF3 mediate maturation of the iron-sulfur subunit of succinate dehydrogenase. Cell Metab 20, 253–266 (2014). [PubMed: 24954417]
17. Michelucci A. et al. Immune-responsive gene 1 protein links metabolism to immunity by catalyzing itaconic acid production. Proc Natl Acad Sci U S A 110, 7820–7825 (2013). [PubMed: 23610393]

18. Mathewson ND et al. Gut microbiome-derived metabolites modulate intestinal epithelial cell damage and mitigate graft-versus-host disease. Nat Immunol 17, 505–513 (2016). [PubMed: 26998764]
19. Suzuki T, Yoshida S. & Hara H. Physiological concentrations of short-chain fatty acids immediately suppress colonic epithelial permeability. Br J Nutr 100, 297–305 (2008). [PubMed: 18346306]
20. Wu SR & Reddy P. Tissue tolerance: a distinct concept to control acute GVHD severity. Blood 129, 1747–1752 (2017). [PubMed: 28153825]
21. Donohoe DR et al. The microbiome and butyrate regulate energy metabolism and autophagy in the mammalian colon. Cell Metab 13, 517–526 (2011). [PubMed: 21531334]
22. Chouchani ET et al. Ischaemic accumulation of succinate controls reperfusion injury through mitochondrial ROS. Nature 515, 431–435 (2014). [PubMed: 25383517]
23. Guzy RD, Sharma B, Bell E, Chandel NS & Schumacker PT Loss of the SdhB, but Not the SdhA, subunit of complex II triggers reactive oxygen species-dependent hypoxia-inducible factor activation and tumorigenesis. Mol Cell Biol 28, 718–731 (2008). [PubMed: 17967865]
24. Lemarie A, Huc L, Pazarentzos E, Mahul-Mellier AL & Grimm S. Specific disintegration of complex II succinate:ubiquinone oxidoreductase links pH changes to oxidative stress for apoptosis induction. Cell Death Differ 18, 338–349 (2011). [PubMed: 20706275]
25. Martinvalet D, Zhu P. & Lieberman J. Granzyme A induces caspase-independent mitochondrial damage, a required first step for apoptosis. Immunity 22, 355–370 (2005). [PubMed: 15780992]
26. Dotiwala F. et al. Granzyme B Disrupts Central Metabolism and Protein Synthesis in Bacteria to Promote an Immune Cell Death Program. Cell 171, 1125–1137 e1111 (2017). [PubMed: 29107333]
27. Walch M. et al. Cytotoxic Cells Kill Intracellular Bacteria through Granulysin-Mediated Delivery of Granzymes. Cell 161, 1229 (2015).
28. Zhang Z. et al. Gasdermin E suppresses tumour growth by activating anti-tumour immunity. Nature 579, 415–420 (2020). [PubMed: 32188940]
29. Lu Y. et al. Caspase-11 signaling enhances graft-versus-host disease. Nat Commun 10, 4044 (2019). [PubMed: 31492850]
30. Humphries F. et al. Succination inactivates gasdermin D and blocks pyroptosis. Science 369, 1633–1637 (2020). [PubMed: 32820063]
31. Luan HH et al. GDF15 Is an Inflammation-Induced Central Mediator of Tissue Tolerance. Cell 178, 1231–1244 e1211 (2019). [PubMed: 31402172]
32. Cooke KR et al. Tumor necrosis factor- alpha production to lipopolysaccharide stimulation by donor cells predicts the severity of experimental acute graft-versus-host disease. J Clin Invest 102, 1882–1891 (1998). [PubMed: 9819375]
33. Hill GR et al. Interleukin-11 promotes T cell polarization and prevents acute graft-versus-host disease after allogeneic bone marrow transplantation. J Clin Invest 102, 115–123 (1998). [PubMed: 9649564]
34. Mathew AV, Seymour EM, Byun J, Pennathur S. & Hummel SL Altered Metabolic Profile With Sodium-Restricted Dietary Approaches to Stop Hypertension Diet in Hypertensive Heart Failure With Preserved Ejection Fraction. J Card Fail 21, 963–967 (2015). [PubMed: 26497755]
35. Campbell EL et al. Transmigrating neutrophils shape the mucosal microenvironment through localized oxygen depletion to influence resolution of inflammation. Immunity 40, 66–77 (2014). [PubMed: 24412613]
36. West AP et al. Mitochondrial DNA stress primes the antiviral innate immune response. Nature 520, 553–557 (2015). [PubMed: 25642965]
37. Chacko BK et al. The Bioenergetic Health Index: a new concept in mitochondrial translational research. Clin Sci (Lond) 127, 367–373 (2014). [PubMed: 24895057]

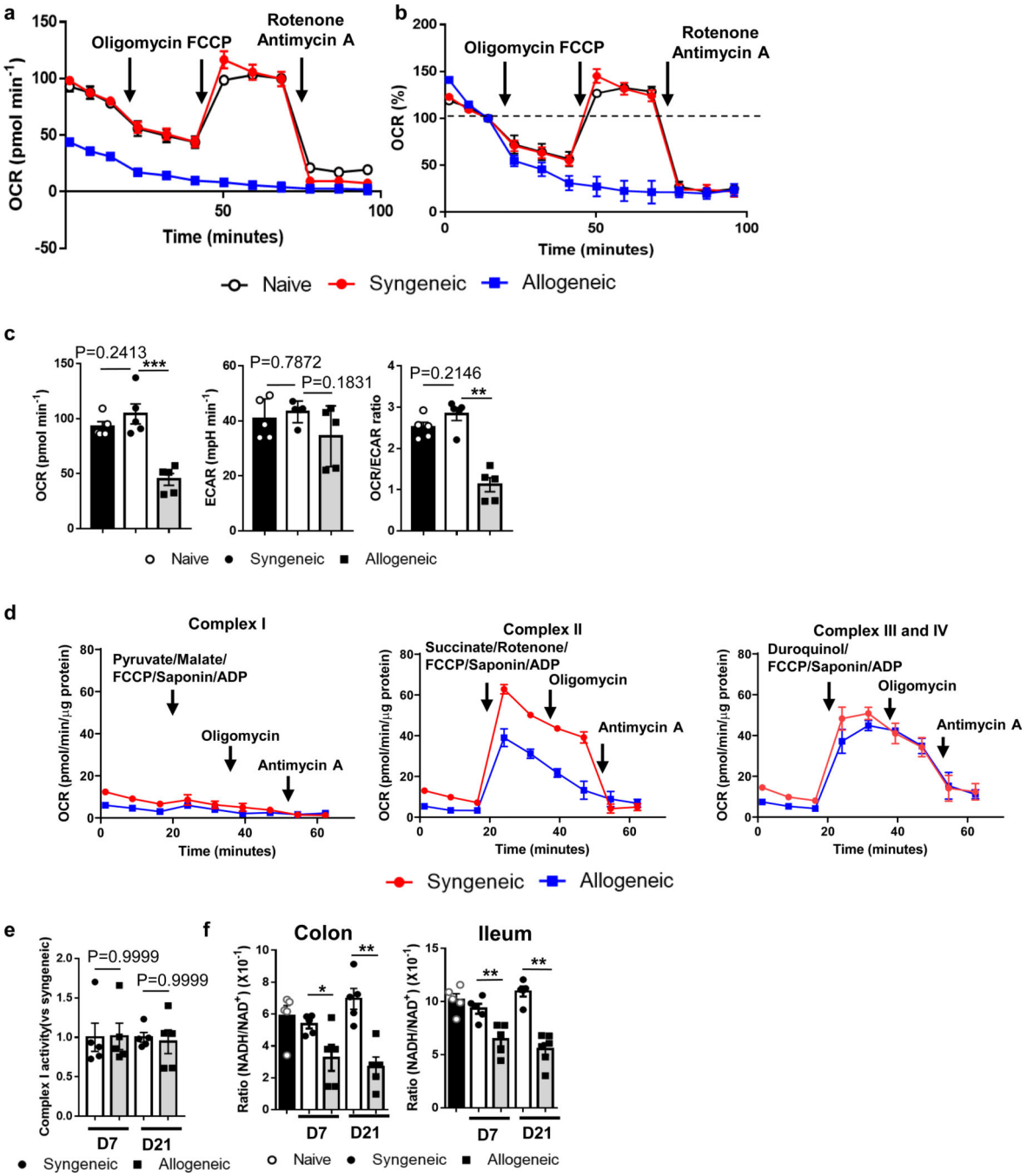

Fig. 1: Mitochondrial respiration in IECs change after allo-HCT.

B6 WT animals received 10 Gy total body irradiation and received 3×10^6 T cells along with 5×10^6 TCD-BM cells from either syngeneic B6 WT or allogeneic MHC-mismatched BALB/c donors. (**a-c**) Representative bio-energetic profiles of naïve, syngeneic or allogeneic isolated IECs on day21 post HCT under basal conditions and following treatment with mitochondrial inhibitors (oligomycin, FCCP, rotenone). (**a**) oxygen consumption rate: OCR, (**b**) % change of OCR from basal conditions, (**c**) basal OCR, extracellular acidification rate (ECAR) and OCR/ECAR ratio (n=5). (**d**) Comprehensive measurement of respiratory

activity in permeabilized IECs. OCR of IECs treated with substrates of complex I (pyruvate/malate), complex II (succinate), or complex III and IV (duroquinol) (n=3). (e) Complex I activity was evaluated in isolated mitochondria of colonic IECs from syngeneic and allogeneic recipients 7 and 21days post HCT (n=5). (**f**) $NADH/NAD^+$ ratio was determined in isolated IECs from naïve, syngeneic, and allogeneic recipients 7 and 21days post HCT (n=5). All data are from biologically independent animals. Representative plots and a graph summarizing the results of at least two independent experiments are shown. One-way ANOVA analysis with Tukey post hoc test (**c**) or two-tailed Mann-Whitney test (**e, f**) (mean ± s.e.m.) were used to determine significance.

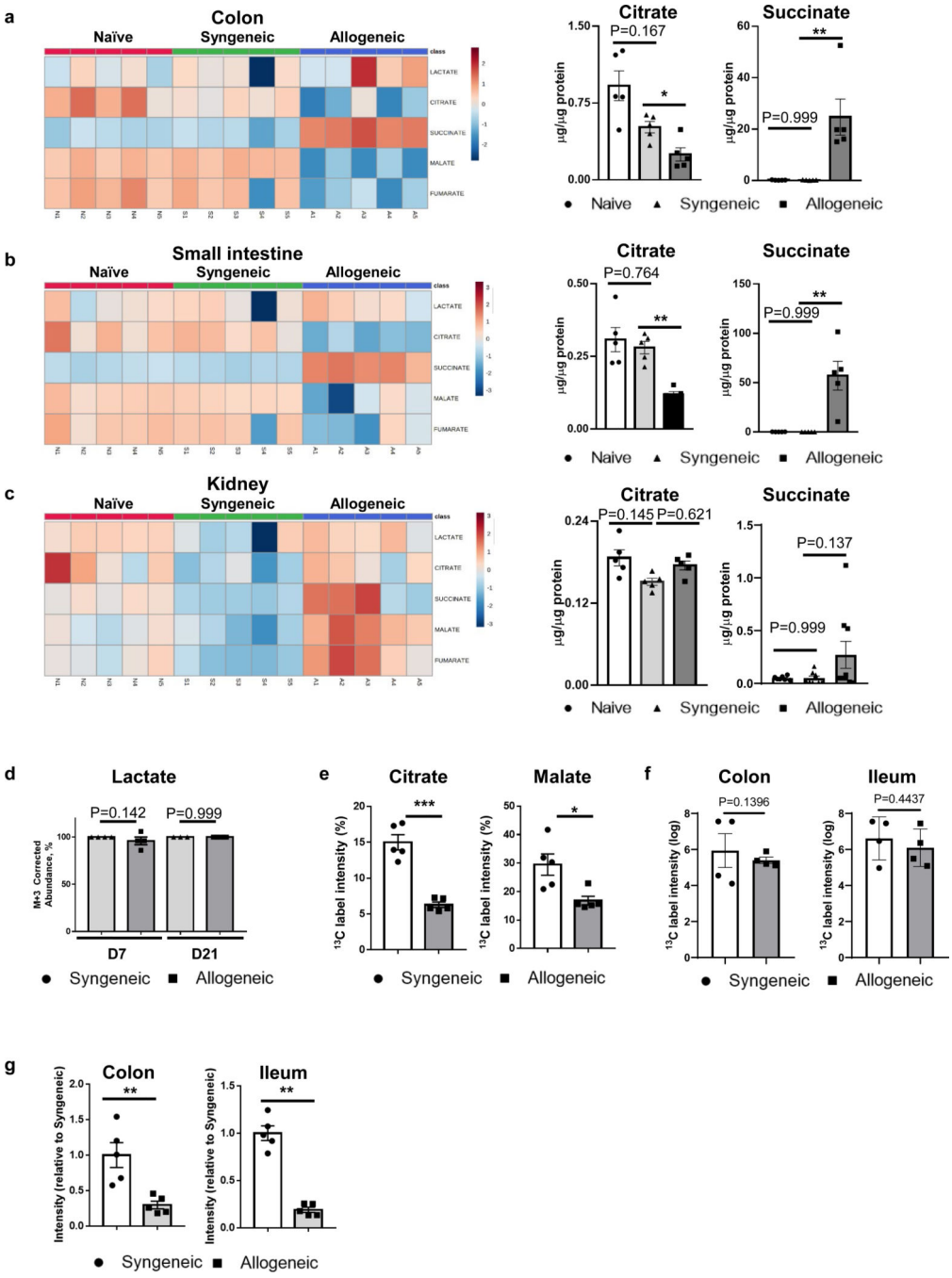

Fig. 2: Increased levels of succinate in IECs post-allo-HCT.

B6 WT animals received 10 Gy total body irradiation and received 3×10^6 T cells along with 5×10^6 TCD-BM cells from either syngeneic B6 WT or allogeneic MHC-mismatched BALB/c donors **(a-c)** Abundance of TCA metabolites on day 21 in colon tissue (**a**), in ileum tissue (**b**) and in kidney cortex (**c**) from syngeneic and allogeneic recipients or naïve mice. The heat maps (left) and graphical results for citrate and succinate (right, colon: n=5, ileum: n=5, kidney: citrate, n=5, succinate, Naïve: n=7; Syn: n=9; Allo: n=9) are shown. (**d**) Abundance from uniformly ^{13}C-glucose in lactate after 4 h in syngeneic or allogeneic

isolated IECs 7 and 21days post HCT (D7 Syn: n=4, Allo: n=4, D21 Syn: n=3, Allo: n=6). (**e**) In vivo Metabolic Flux analysis of colon from ^{13}C-glucose treated mice 7days post HCT. The percentage of ^{13}C label intensity in citrate and malate in small and large intestine (n=5). (**f**) In vivo Metabolic Flux analysis from ^{13}C-palmitate treated mice colon and small intestine 7days post HCT (n=4). The log transformed ^{13}C label intensity in succinate in colon and ileum. (**g**) Intensity of SDH enzyme activity staining from colon and ileum 21days post HCT (n=5). All data are from biologically independent animals. Representative plots and a graph summarizing the results of at least two independent experiments are shown. One-way ANOVA analysis with Tukey post hoc test (**a**-**c**), two-tailed unpaired t-test (**d, e, f**) or two-tailed Mann-Whitney test (**g**) (mean ± s.e.m.) were used to determine significance.

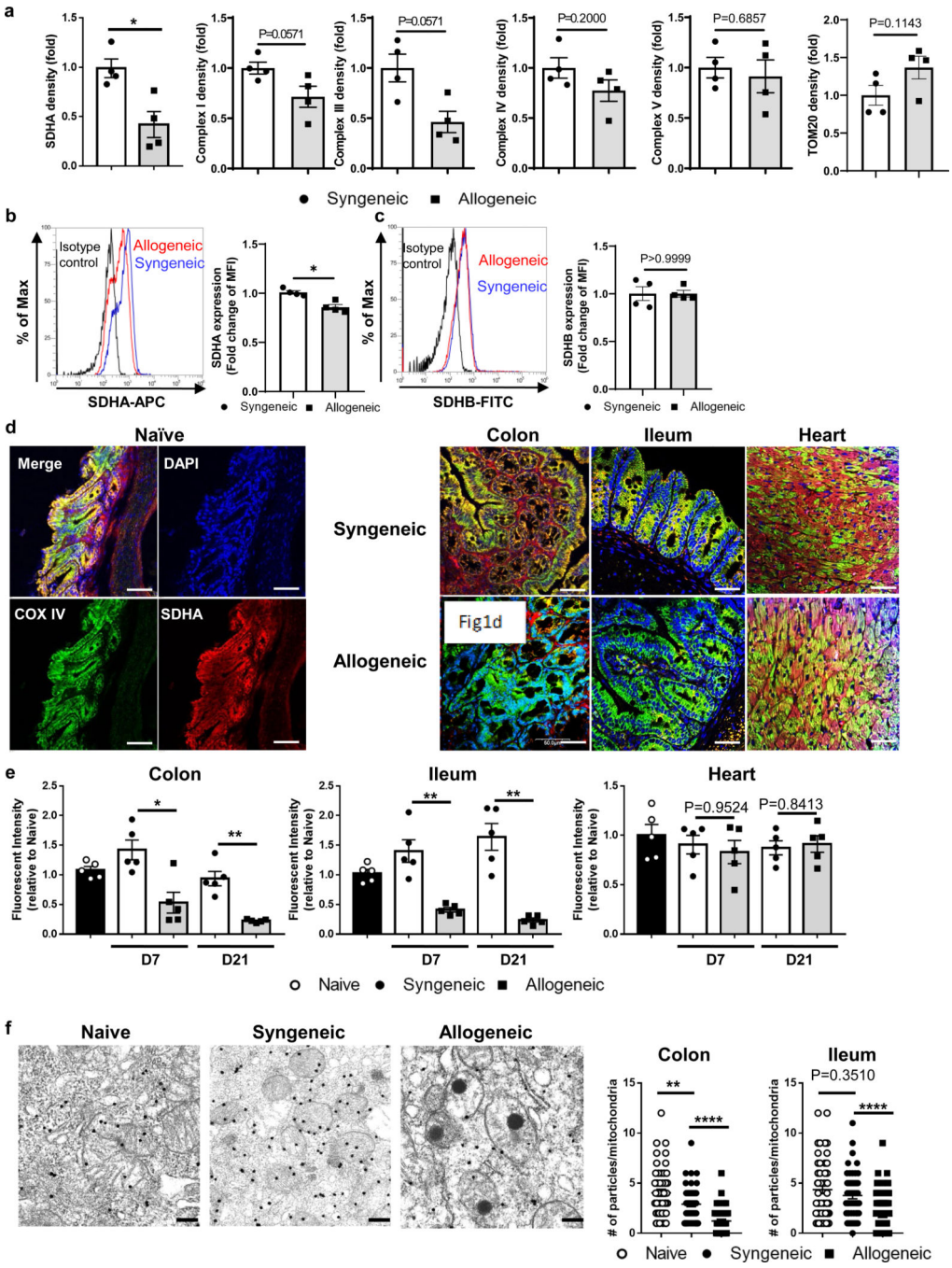

Fig. 3: Reduction of SDHA protein levels in IECs post allo-HCT.

B6 WT animals received 10 Gy total body irradiation and 3×10^6 T cells along with 5×10^6 TCD-BM cells from either syngeneic B6 WT or allogeneic BALB/c donors. (**a**) Immunoblot protein density quantification of SDHA, complex I, III, IV, V and TOM-20 in mitochondria from IECs 21days post HCT (n=4). Immunoblot image is shown in Extended Data Fig. 3a.. (**b, c**) SDHA and SDHB expression of CD326 positive IECs 7days post HCT were measured by flow cytometry. Representative flow cytometry image of SDHA (**b**, left) and SDHB (**c**, left), SDHA expression levels (**b**, right) and SDHB expression levels (**c**, right) were shown

(n=4). (**d**) Representative images of immunofluorescence staining of colon, ileum and heart from naïve or recipients 21days post HCT (Complex IV=green, SDHA=red, DAPI=blue, scale bar= 50 μm, n=5). (**e**) Fluorescent intensity of SDHA in colon, ileum and heart from naïve, syngeneic or allogeneic recipients 21days post HCT (n=5). (**f**) Representative images of transmission electron microscopy with immune-gold staining for SDHA in mitochondria of colon from naive mice or recipients 21days post HCT (left; scale bar 200nm) and numbers of gold particles per mitochondrial in colon and ileum 21days post HCT (right) (50 mitochondria from 3 samples). Data **(a-e)** are from biologically independent animals. Representative plots and a graph summarizing the results of at least two independent experiments are shown. Two-tailed Mann-Whitney test (**a, b, c, e**) or one-way ANOVA analysis with Tukey post hoc test (**f**) were used to determine significance(mean ± s.e.m.).

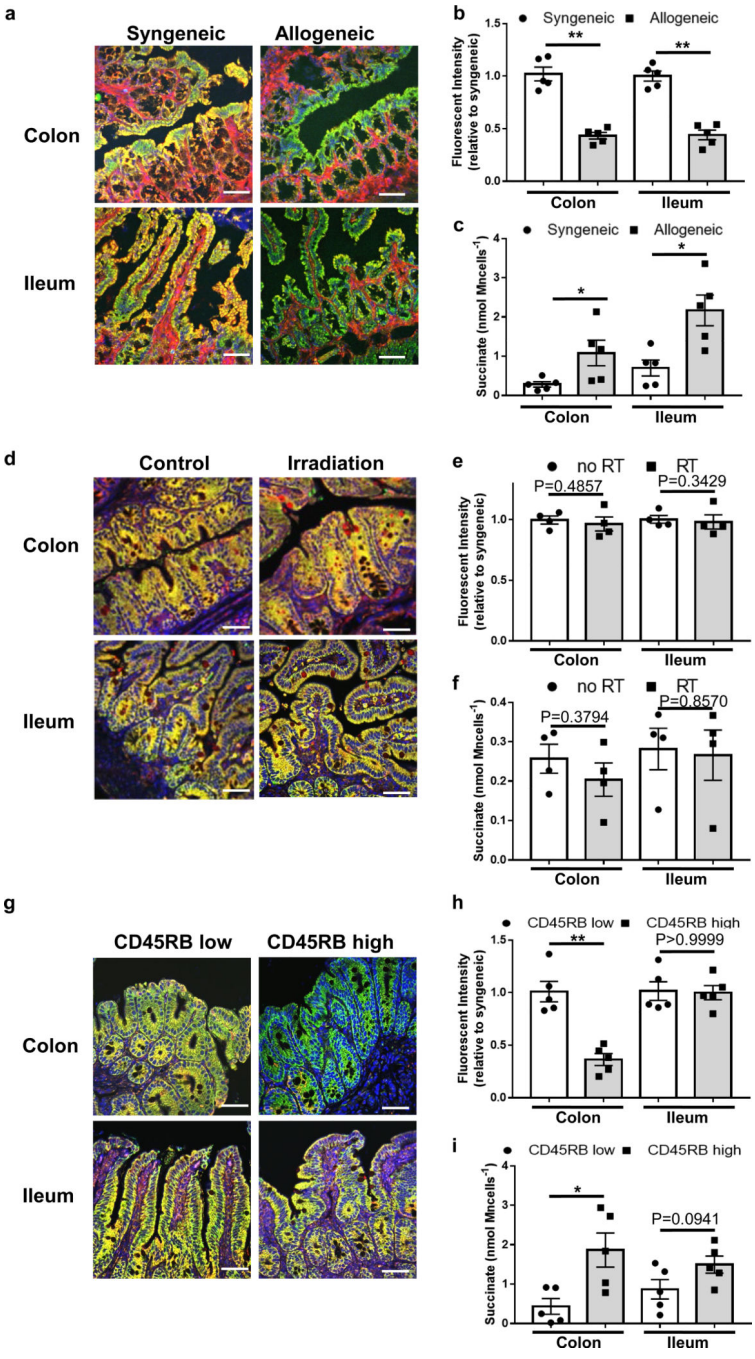

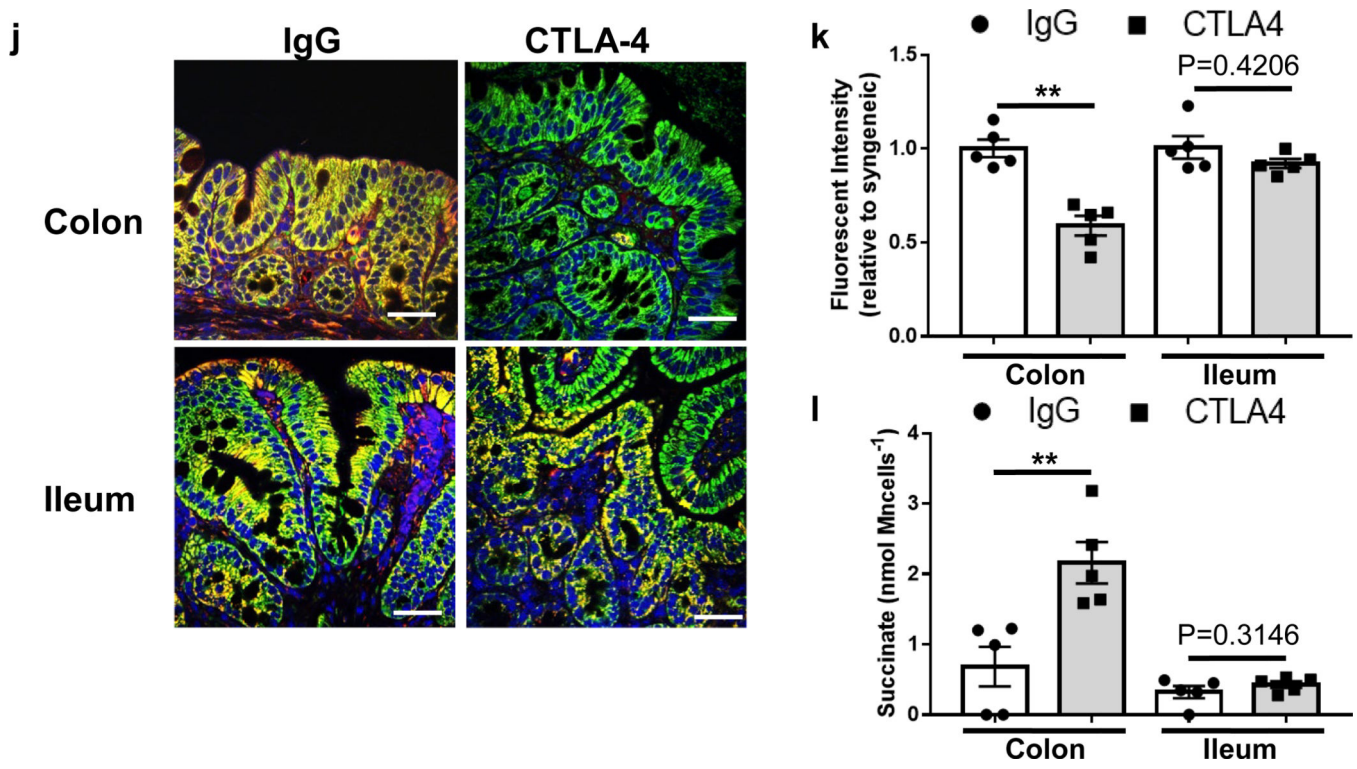

Fig. 4: T-cell mediated intestinal immunopathology and SDHA reduction in IECs.

(a-c) Unirradiated B6D2F1 mice received 10×10^7 splenocytes from syngeneic B6D2F1 or allogeneic B6 WT donors (n=5). (**a**) Representative images of immunofluorescence staining and (**b**) fluorescent intensity of SDHA in colon and ileum from B6D2F1 recipients 21days post HCT (scale bar= 50 μm). (**c**) Succinate levels in isolated IECs from colon and ileum 21days post HCT. (**d-f**) B6 WT mice received 10 Gy total body irradiation without T-cell or BM cells (n=4). (**d**) Representative images of immunofluorescence staining and (**e**) fluorescent intensity of SDHA in colon and ileum from irradiated or non-irradiated (control) mice 9days post irradiation (scale bar= 50 μm). (**f**) Succinate levels in isolated IECs from colon and ileum 9days post irradiation. (**g-i**) $CD4^+CD25^-CD44^-CD45RB^{hi}$ (naïve) T cells or $CD4^+CD25^-CD44^-CD45RB^{low}$ (non-naïve) T cells from B6 WT mice were transferred to RAG-$1^{-/-}$ mice (n=5). (**g**) Representative images of immunofluorescence staining and (**h**) fluorescent intensity of SDHA in colon and ileum 8 weeks after induction of colitis (scale bar= 50 μm). (**i**) Succinate levels in isolated IECs from colon and ileum at 8 weeks after T cell transfer. (**j-l**) B6 WT mice receiving isotype control IgG or anti-CTLA-4 antibody were treated with 3% DSS in drinking water for 7 days (n=5). (**j**) Representative images of immunofluorescence staining and (**k**) fluorescent intensity of SDHA in colon from mice receiving IgG or CTLA-4 antibody 12days after DSS treatment (scale bar= 50 μm). (**l**) Succinate levels in isolated IECs from colon and ileum 12days after 3% DSS administration. All Data are from biologically independent animals. Representative plots and a graph summarizing the results of at least two independent experiments are shown. Two-tailed Mann-Whitney test (**b, e, h, k**) or two-tailed unpaired t-test (**c, f, i, l**) (mean ± s.e.m.) were used to determine significance.

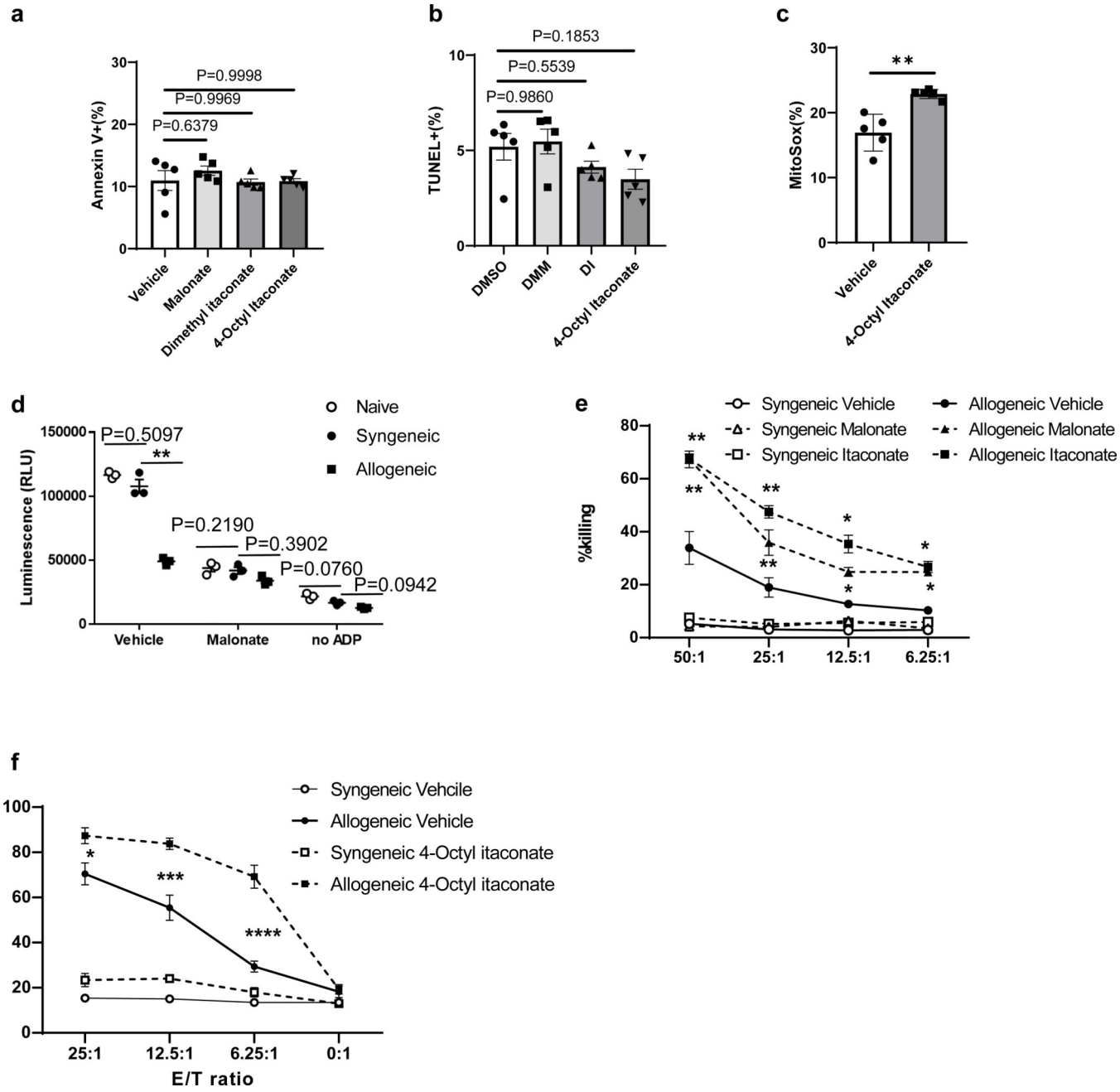

Fig. 5: Functional relevance of SDHA reduction in IECs.

(**a-c**) Primary colonic epithelial cells **(**PCECs) were treated with DMSO, malonate, itaconate or 4-Octyl itaconate for 6 hours (n=5 cells examined over 3 independent experiments). (**a**) Representative images and annexin-V positive cells are shown. (**b**) Tunel positive cells are shown. (**c**) MitoSox positive cells are shown. (**d**) B6 WT animals received 10 Gy total body irradiation and received 3×10^6 T cells along with 5×10^6 TCD-BM cells from either syngeneic B6 WT or allogeneic BALB/c donors. ATP production in isolated mitochondria of colon from naïve, syngeneic and allogeneic recipients 21days post HCT (n=3 biologically independent animals). Mitochondria were treated with vehicle, malonate or vehicle without

ADP. (**e**) Isolated splenic T cells from either syngeneic B6 WT or allogeneic BALB/c animals were cultured with irradiated splenocytes derived from B6 WT animals for 96 hours, and $CD8^+$ T cells were purified as effector cells. PCECs from B6 WT animals were treated with vehicle, malonate or itaconate and used as targets for effector T-cells. In vitro allogeneic cytotoxic assay (CTL assay) with 51Cr using effector cells against PCECs was analyzed (data are from 1 of 4 similar experiments). (**f**) PCECs were treated with vehicle or 4-Octyl itaconate (0.2mM) for 2hours and used as targets for effector T-cells. Cell death was analyzed (data are from 1 of 4 similar experiments). One-way ANOVA analysis with Tukey post hoc test (**a, b, d, e, f**) or two-tailed unpaired t-test (**c**) (mean ± s.e.m.) were used to determine significance.

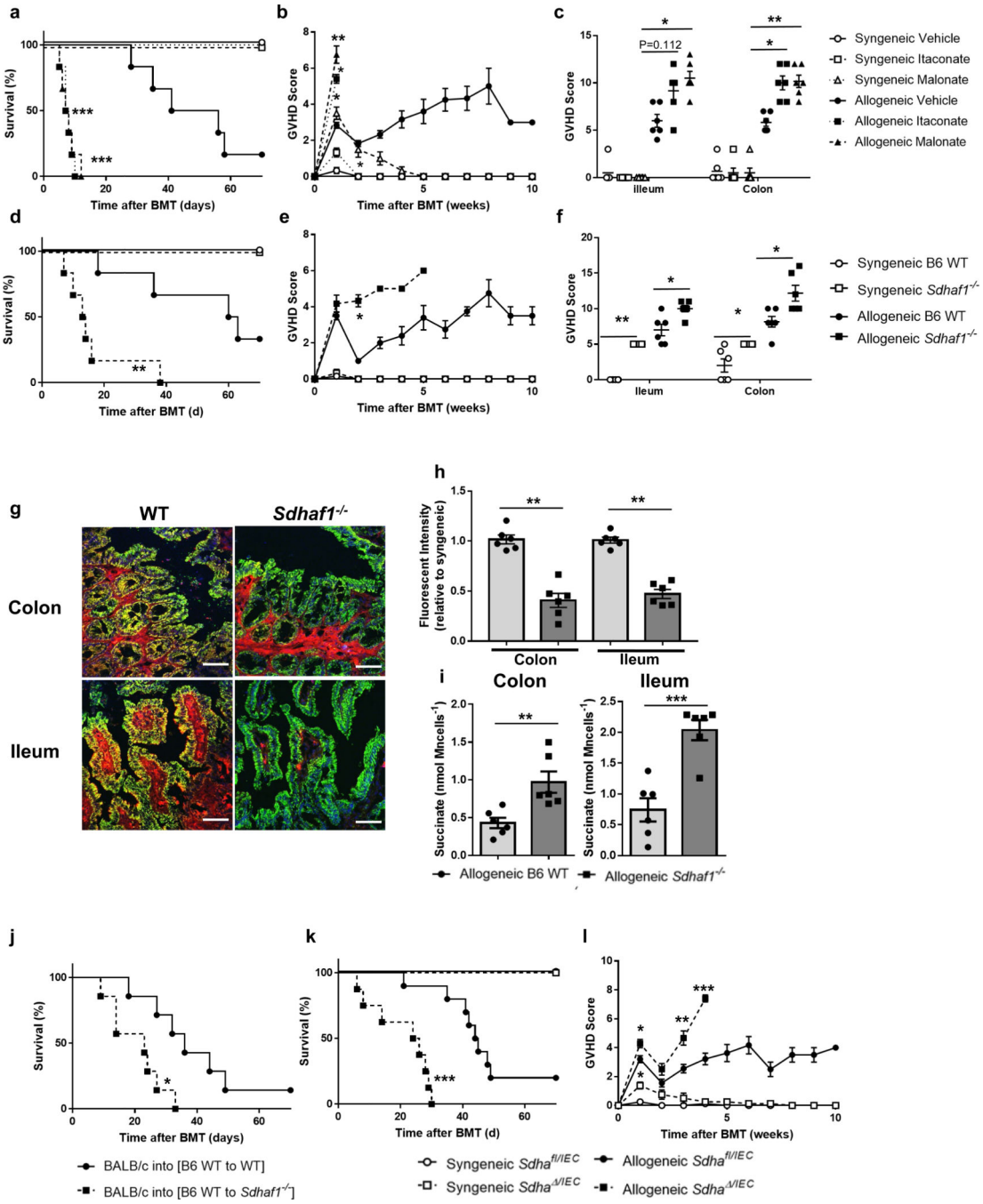

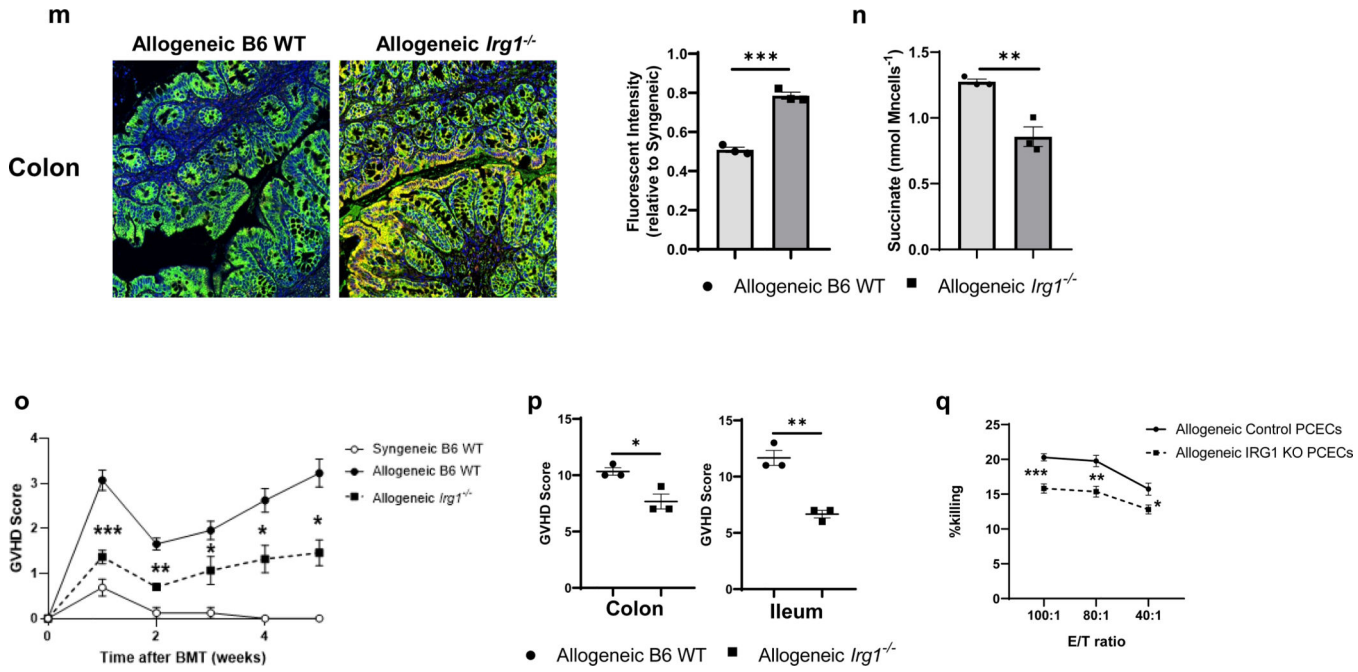

Fig. 6: SDHA in IECs regulates the severity of GVHD.

B6 WT, *Sdhaf1*$^{-/-}$, *Sdha*$^{\Delta/IEC}$ or *Sdha*$^{fl/IEC}$ animals received 10 Gy total body irradiation followed by 3×10^6 T cells and 5×10^6 TCD-BM cells from either syngeneic B6 WT or allogeneic BALB/c donors. (**a-c**) B6 WT recipients were treated with vehicle, malonate (5g kg^{-1}) or itaconate (2.5g kg^{-1}) every other day post HCT. Survival (**a**), clinical GVHD severity (**b**) and pathological GVHD scores in ileum and colon 7days post HCT (**c**) (n=6). (**d-f**) B6 WT and *Sdhaf1*$^{-/-}$ mice received HCT (n=6). Survival (**d**), clinical GVHD severity (**e**) and pathological GVHD scores in ileum and colon 7days post HCT (**f**). (**g**) Representative images of immunofluorescence staining and (**h**) fluorescent intensity of colon and ileum from B6 WT and *Sdhaf1*$^{-/-}$ mice 7days post allo-HCT (Complex IV=green, SDHA=red, DAPI=blue, scale bar= 50 μm, n=6). (**i**) Succinate levels in isolated IECs from colon and ileum of B6 WT and *Sdhaf1*$^{-/-}$mice at day7 post allo-HCT (n=6). (**j**) Survival of chimeric [B6 Ly5.2→B6 WT] and [B6 Ly5.2→ *Sdhaf1*$^{-/-}$] animals receiving 9 Gy TBI followed by 3×10^6 T cells and 5×10^6 TCD-BM cells from syngeneic B6 WT or allogeneic BALB/c donors. (**k**) Survival and clinical GVHD severity (**l**) of *Sdha*$^{\Delta/IEC}$ and *Sdha*$^{fl/IEC}$ mice post HCT (syngeneic *Sdha*$^{\Delta/IEC}$ and *Sdha*$^{fl/IEC}$: n=6, allogeneic *Sdha*$^{\Delta/IEC}$: n=8, allogeneic *Sdha*$^{fl/IEC}$: n=10). All Data are from biologically independent animals. Representative plots and a graph summarizing the results of at least two independent experiments are shown. All statistical analysis by log-rank test (**a, d, j**), two-tailed Mann-Whitney test (**b, e, f, h, l**), Kruskal-Wallis analysis with Dunn's post hoc test (**c**) or two-tailed unpaired t-test (**i**) (mean ± s.e.m.).

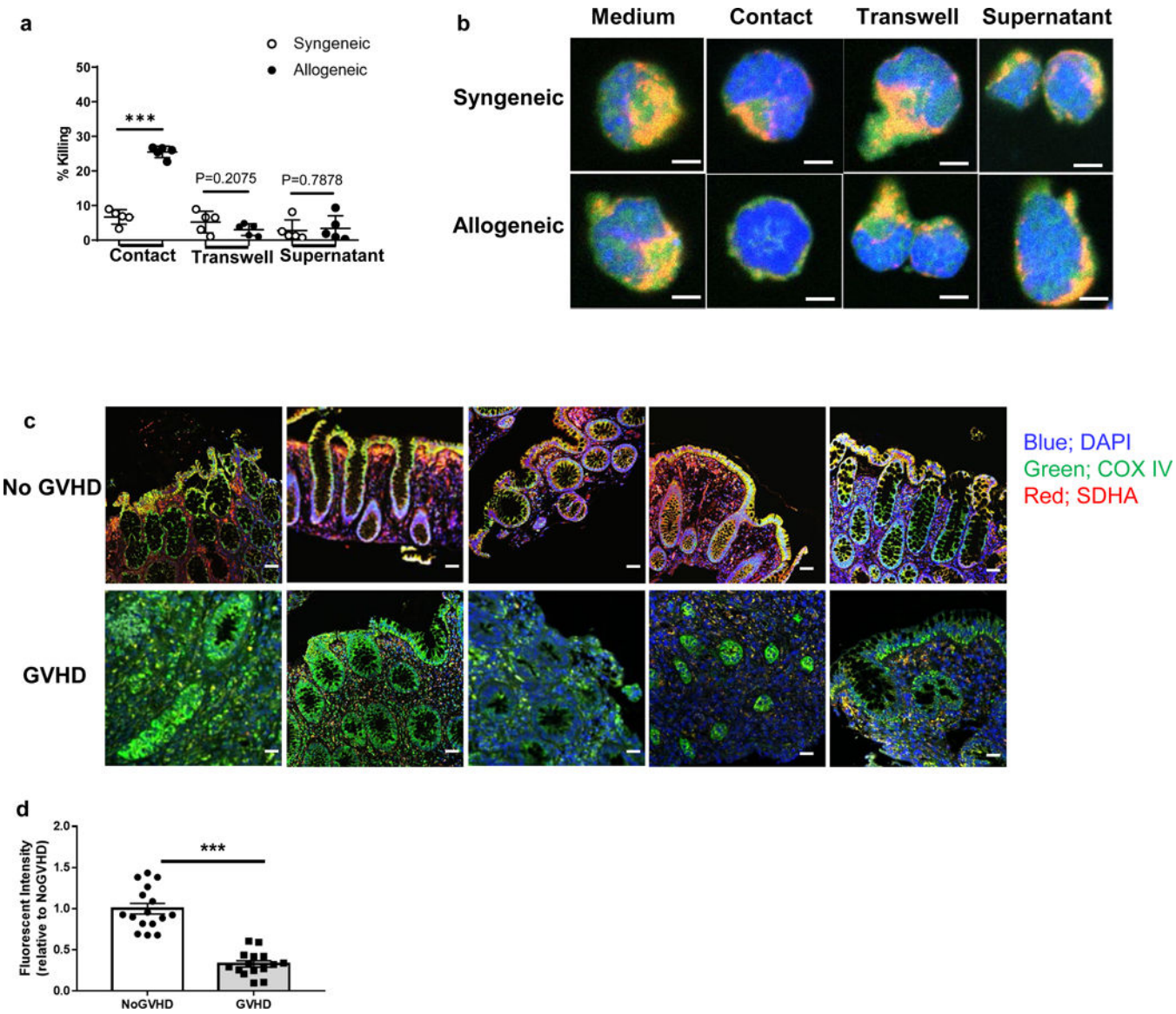

Fig.7: Contact by T cells induce cell death of IECs.

(**a**) Isolated splenic T cells from either B6 WT or BALB/c mice were cultured with irradiated splenocytes derived from B6 WT for 96 hours and $CD8^+$ T cells were purified as effector cells. 51Cr-release assay using effector cells against PCECs was determined in direct or indirect co-culture with T-cells (using transwell membrane) or supernatant treatment from effector cell culture for 4hours (n=5). Three independent experiments were performed with similar results. (**b**) Representative images of immunofluorescence staining of $CD326^+$ PCECs from T cell treatment as shown in (**a**) (Complex IV=green, SDHA=red, DAPI=blue, scale bar= 5μm, n=5 biologically independent animals). (**c-d**) Representative images of immunofluorescence staining of colonic biopsy samples from patients clinically suspected to have lower GI GVHD after allo-HCT (**c**, Complex IV=green, SDHA=red, DAPI=blue scale bar= 50 μm, GVHD: n=15, non-GVHD: n=16) and (**d**) Integrated

fluorescent intensity of SDHA levels. Two-tailed unpaired t-test (**a, d**) (mean ± s.e.m.) were used to determine significance.

Table 1:

β-oxidation activity in IECs after HCT.

Tissue acylcarnitine	Syngeneic	Allogeneic	P value
Small Intestine	μM	μM	
C2	1404±376	1197±505	0.54
C4	30±8	42±7	0.07
C8	0.13±0.09	0.14±0.02	0.71
C16	260±83	239±83	0.74
Large Intestine			
C2	1370±88	1532±223	0.23
C4	142±32	234±107	0.15
C8	0.09±0.1	0.09±0.05	0.97
C16	41±41	14±8	0.24

Acylcarnitine levels in colon and ileum from naïve, syngeneic or allogeneic recipients 21day post HCT (n=4 biologically independent animals). Statistical analysis by two-tailed unpaired t-test (mean ± s.d.) were used to determine significance.